Journal of Human Evolution 217 (2026) 103855

Contents lists available at ScienceDirect

Journal of Human Evolution

journal homepage: www.elsevier.com/locate/jhevol

Dental morphology and ancient human dispersals within and out of Africa

Joel D. Irish [a, b, *], Adeline Morez Jacobs [a, c], James M. Lea [d], Linus Girdland Flink [a, e], G. Richard Scott [f]

[a] School of Biological and Environmental Sciences, Liverpool John Moores University, Liverpool, L3 3AF, UK
[b] Centre for the Exploration of the Deep Human Journey, University of the Witwatersrand, Private Bag 3, WITS 2050, South Africa
[c] Dipartimento di Biologia, Università Degli Studi di Padova, Via U. Bassi, 58/B – 35121, Italy
[d] Department of Geography and Planning, School of Environmental Sciences, University of Liverpool, Liverpool, L69 7ZT, UK
[e] Department of Archaeology, School of Geosciences, University of Aberdeen, Aberdeen, AB24 3UF, UK
[f] Anthropology Department, University of Nevada Reno, Reno, NV, 89557, USA

ARTICLE INFO

Article history:
Received 5 January 2026
Accepted 10 May 2026
Available online xxx

Keywords:
Arizona State University Dental Anthropology System
Minimum-slope geographic distances
Out-of-Africa II
Isolation by distance
Serial founder effect
Population history

ABSTRACT

We used traits from the Arizona State University Dental Anthropology System (ASUDAS) to investigate the Out-of-Africa II dispersal (~70,000–50,000 BP) and biogeographic dynamics within the continent since the Late Pleistocene. Mean measure of divergence (MMD) distances from 32 recent global and five Early-Late Holocene African dental samples (n = 3167 individuals) were compared with F_{ST} distances from matched genetic samples (n = 566), serving as an independent line of validation. We then incorporated multidimensional scaling (MDS), Mantel correlations, linear regression, and novel minimum-slope geographic distances to reconstruct global population structure. Strong correlations ($r_m > 0.7$) resulted between MMD and F_{ST} matrices and between the latter and their respective minimum-slope distances. The dental and genetic MDS plots revealed the patterning characteristic of seriated spatial or temporal data, indicating greater diversity within Africa than outside of it. Inclusion of the ancient samples revealed long-term phenetic continuity in East and South Africa and a south-north gradient in dental variation. Regressing MDS coordinates against minimum-slope distances yielded the highest R^2 value for recent and ancient South African samples (≤0.86), mirroring genetic clines linked with deep Pleistocene structure and Holocene population movements. These findings are consistent with isolation by distance and compatible with serial founder processes associated with the Late Pleistocene dispersal from East Africa. They also suggest Sub-Saharan Africans had formed regionally structured but interconnected populations throughout the Holocene, with South African groups retaining high diversity and features reflecting deep ancestry. Overall, the ASUDAS traits broadly track population history and patterns observed in neutral genomic structure.

1. Introduction

Multidisciplinary research continues to enhance our understanding of modern human origins and their global expansion. In particular, genetic studies have yielded new insights into population structure and mobility. That said, analyses of skeletal morphology, notably dental variation, offer an independent and temporally deeper source of evidence. Here, we used nonmetric traits in the Arizona State University Dental Anthropology System (ASUDAS) (Turner et al., 1991; Scott and Irish, 2017) to examine the Late Pleistocene dispersal from Africa and biogeographic dynamics within the continent.

Our previous work (Irish et al., 2020) demonstrated that ASUDAS traits, some with narrow-sense heritability estimates of 0.60–0.93 (Higgins et al., 2009; Hughes and Townsend, 2011, 2013; Hughes et al., 2016), preserve information about population structure in a broadly comparable way to neutral genomic markers. Using matched global dental and genomic datasets, strong correspondence was observed between phenetic and genetic distances.

In that study, Mantel correlations between mean measure of divergence (MMD) distances from 25 ASUDAS traits and Hudson's F_{ST} from 353,090 single nucleotide polymorphisms (SNPs) returned strong r_m values of 0.84 and 0.72 ($p < 0.01$) in 12 matched

* Corresponding author.
E-mail address: J.D.Irish@ljmu.ac.uk (J.D. Irish).

https://doi.org/10.1016/j.jhevol.2026.103855

Figure 1. Geographic locations of 32 recent dental and matched genetic samples from our previous work (Irish et al., 2020) and present study. See text and Tables 1 and 2 for details. (For interpretation of the references to color in this figure, the reader is referred to the web version of this article.)

African and 32 global samples, respectively. Matching (Fig. 1) was based on shared geographic, language, and ethnic backgrounds. Stronger correlations would be expected if dental and genetic data were from the same individuals. Both MMD and F_{ST} matrices correlated strongly with great-circle straight-line geographic distances ($r_m > 0.7$), supporting isolation by distance (IBD) (Wright, 1943; Relethford, 2004). Multidimensional scaling (MDS) of the dental and genetic data revealed spatial patterns consistent with an expansion from Africa—beginning with Sub-Saharan groups located on the left of dimension 1 in Figure 2 (also Supplementary Online Material [SOM] Fig. S1), with subsequent differentiation among populations proceeding around the plot—indicating that ASUDAS traits can approximate patterns observed in DNA data when the latter are unavailable (Irish et al., 2020).

Irish (1997:463) first noted that phenetic distances among global dental samples detect 'an expansive dental morphological cline' emanating from Africa, as revisited by Hanihara (2013) and Reyes-Centeno et al. (2017) in the context of the Out-of-Africa II dispersal. Initiating ~70,000–50,000 BP (Soares et al., 2012; Malaspinas et al., 2016; Pagani et al., 2016; Bergström et al., 2021; Hallett et al., 2025), it extended across Arabia, into southern Asia, and Sahul by ~65,000–40,000 BP (Garcea, 2010; Clarkson et al., 2017; Langgut et al., 2018; Ponce de León et al., 2018; Beyer et al., 2021; Hublin, 2021; Abbas et al., 2023; Saltré et al., 2024), reaching Europe by the end of this time (Hublin et al., 2020), and the Americas afterward (Moreno-Mayar et al., 2018). Relative to non-Africans, Sub-Saharan populations share a suite of distinct mass-additive traits (Irish, 1997), though with higher regional variation. With exception (mentioned later), this variation decreases at greater distances from the subcontinent (Irish, 1998a; Irish and Guatelli-Steinberg, 2003), paralleling the reduction in global genetic diversity widely interpreted as indicative of serial founder effects (Prugnolle et al., 2005; Ramachandran et al., 2005; Li et al., 2008; Jay et al., 2013; Kanitz et al., 2018; Tobler et al., 2023). While clinal patterns are expected under serial founder processes, they are not unique to that model and may also arise under broader scenarios of IBD and spatially structured populations.

Here, we extended our previous analyses, starting with the same ASUDAS traits, samples, and model-free approach (Irish et al., 2020) as a baseline, to further resolve this dispersal. Specifically, we incorporate a novel geographic framework and a temporal dimension through Holocene samples. Multidimensional scaling coordinates from MMD distances (c.f., Ponce de León et al., 2018) were regressed against 'minimum-slope' geographic distances to reconstruct global population structure. That is, for geographic distances, we effected an approach that calculates the lowest cumulative surface slope distances among sample origin sites. It explicitly accounts for major topographic features while implicitly incorporating geographic separation. We then evaluated how well these assorted data resolve population structure and regional exchange in Africa since the Pleistocene. This included assessing contributions from East Africa (Ramachandran et al., 2005; Kanitz et al., 2018; Lipson et al., 2022) while acknowledging broader pan-African and weakly structured population models (Bergström et al., 2021) and enduring biocultural influences from South Africa (Wang et al., 2020; Fan et al., 2023), along with more recent documented population movements (Montinaro et al., 2017; Rito et al., 2019; Wang et al., 2020; Sengupta et al., 2021).

To validate these results, equivalent analyses were conducted with F_{ST} distances from our matched genetic samples. We next included a number of 'ancient' Early to Late Holocene dental and genetic samples from East and South Africa to add a temporal

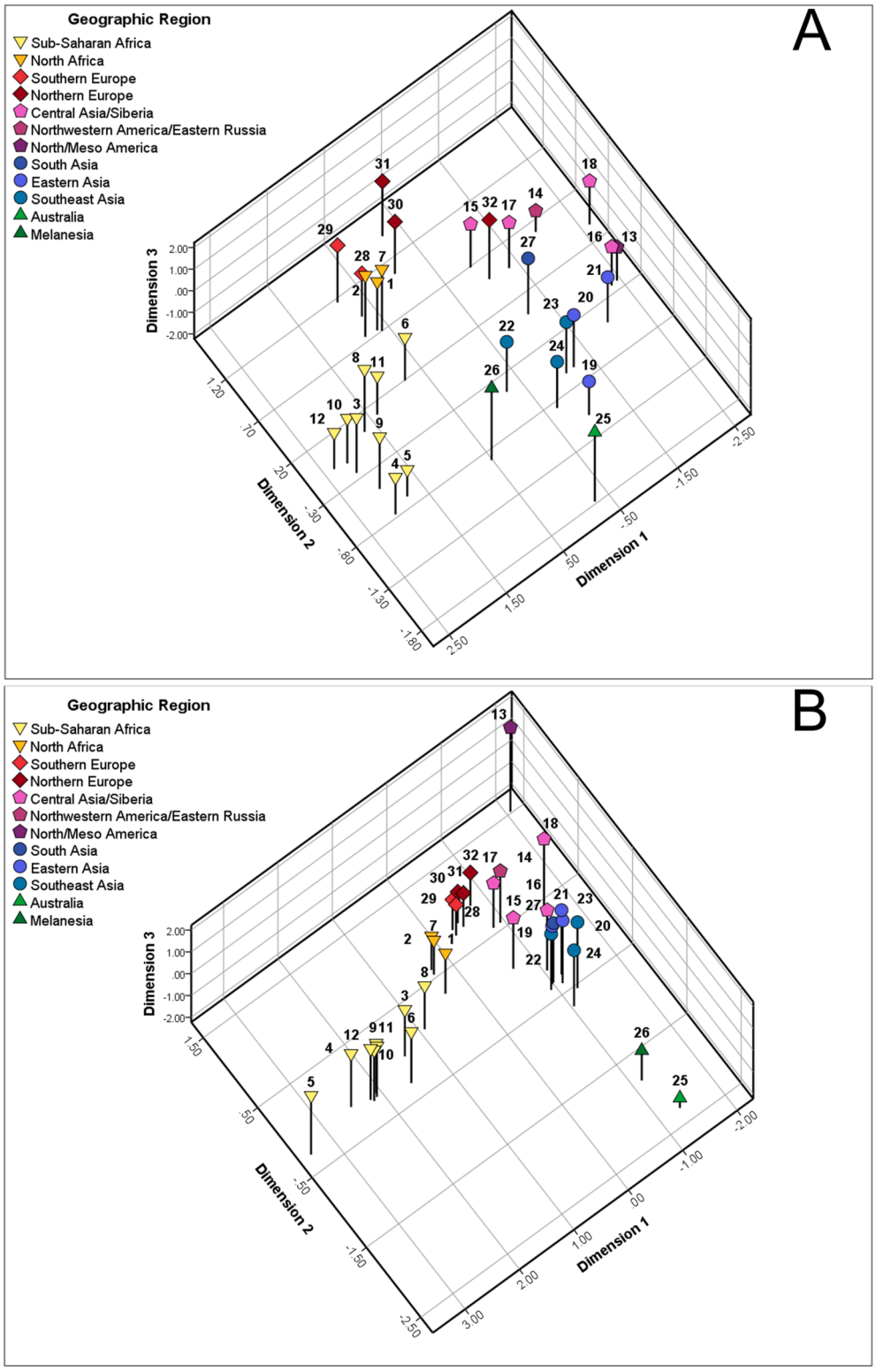

Figure 2. A) Multidimensional scaling plot of MMD distances among 32 recent global dental samples. Sample numbers refer to abbreviations (e.g., 1 = D1_BED) in Table 1. B) Multidimensional scaling plot of F_{ST} distances among 32 recent global genetic samples. Sample numbers refer to abbreviations in Table 2 (e.g., 1 = G1_MOR). Modified from Irish et al. (2020). Details in text and SOM Tables S1–S4. MMD = mean measure of divergence. (For interpretation of the references to color in this figure, the reader is referred to the web version of this article.)

dimension (Konigsberg, 1990; Duforet-Frebourg and Slatkin, 2016; Ponce de León et al., 2018). The ancient genetic samples are not used as a primary basis for reconstructing population history. Instead, they are included as an independent line of comparison to evaluate whether patterns from dental morphology are largely consistent with the genomic data, given current limitations in ancient DNA (aDNA) datasets from Africa.

Our overarching aim is to elucidate the spatial and temporal dynamics of the Out-of-Africa II dispersal based on phenetic, genetic, and geographic evidence. Specifically, we examined how nonmetric dental variation reflects large-scale population structure also observed in genetic data, whether these patterns discern regions of influence and origin within Africa, and if the Holocene samples show diachronic continuity with their recent, regional counterparts. Dental traits provide an independent way to reconstruct population history while complementing the findings from genetics, archaeology, paleogeography, and other pertinent fields. Together, these approaches allow evaluation of both global dispersal patterns and regional population dynamics within Africa. Along these lines, we address three main questions:

1. Do MMD distances from ASUDAS traits correlate with F_{ST} from SNP data in both recent and ancient samples?
2. Within Africa, do Holocene East and South African samples show phenetic continuity with recent populations, indicating long-term stability and intermittent gene flow?
3. Does a south-north gradient in African dental variation parallel known genetic clines?

2. Materials and methods

2.1. Dental and genetic samples

Background for the 32 recent dental ($n = 2844$ individuals) and genetic ($n = 530$) matched samples is summarized in Tables 1 and 2. For the sets of 12 matched African samples, three are from the north and nine from the south of the Sahara. Data are mostly from the youngest samples in the dental dataset, 19th–20th centuries, to best parallel the SNP data in modern individuals (Table 2). The 20 matched non-African samples from Europe, Asia, Australia,

Table 1
The 32 recent dental samples from Irish et al. (2020) used in the present study with background information.

Dental sample	Abbreviation	Region	Country/area	Data source	*n*	Lat	Lon
Africa							
Bedouin (Arab)	D1_BED	North Africa	Morocco and Algeria	Irish (1993, 1998a)	49	34.8	−5.2
Kabyle (Berber)	D2_KAB	North Africa	Algeria	Irish (1993, 1998a)	32	36.6	3.7
Kikuyu	D3_KKU	East Africa	Kenya	Irish unpublished	60	−0.3	36.1
Riet River (San; >12–19th century)[a]	D4_RRI	South Africa	South Africa	Irish et al., (2014) [b]	66	−29.3	24.8
San	D5_SAN	South Africa	Botswana, South Africa	Irish (1993, 1997)	99	−22.4	24.6
Senegambia (Wolof)	D6_SEN	West Africa	Senegambia	Irish (1993, 1997)	42	15.2	−16.7
Shawia (Berber)	D7_SHA	North Africa	Algeria	Irish (1993, 1998a)	26	35.4	6.7
Somalia	D8_SOM	East Africa	Somalia	Irish (2010)	77	9.0	46.4
Sotho	D9_SOT	South Africa	South Africa	Irish (2016)	66	−29.4	28.3
Tswana	D10_TSW	South Africa	South Africa	Irish (2016)	63	−25.8	23.0
Yoruba	D11_YOR	West Africa	Benin (Dahomey)	Irish unpublished	28	6.6	2.6
Zulu	D12_ZUL	South Africa	South Africa	Irish (2016)	67	−28.0	32.4
				Total	**675**		
America, Asia, Australia, Melanesia, Europe							
Pima 94	D13_PIM	North America	Salt River—Maricopa, Arizona	Turner unpublished	165	33.3	−111.5
Aleut (Western US)	D14_ALE	North America	Attu, Atka plus Western Aleut Historic	Turner unpublished; Scott and Irish (2017)	95	52.0	−174.0
Kazak 94 (17–19th century)[a]	D15_KAZ	Central Asia	East Kazakhstan	Turner unpublished	204	47.0	76.0
Mongol 2 and 3 pooled	D16_MON	Central Asia	Northeast Mongolia	Turner unpublished, 1990	82	48.0	110.0
Lower Ob Khanty	D17_LOK	Central Asia	Khant-Mansi (Ugrian), Central Russia	Turner unpublished	49	63.0	70.0
Chukchi plus Eastern Siberia	D18_CHU	Central Asia	Northeast Russia	Turner unpublished	126	67.5	170.0
Recent Thailand	D19_THA	East Asia	Central Thailand	Turner unpublished, 1990	189	13.0	101.0
Recent Tonkin, historic Annam	D20_VIE	East Asia	North Vietnam	Turner unpublished	76	20.0	107.0
Recent Japanese	D21_JAP	East Asia	Central Japan	Turner unpublished; Scott and Irish (2017)	131	36.0	138.0
Malay Composite	D22_MAL	Southeast Asia	Central Malaysia	Turner unpublished; Scott and Irish (2017)	58	1.0	102.5
Philippines no 2 Calatagan BP	D23_PHI	Southeast Asia	Central Philippines	Turner unpublished; Scott and Irish (2017)	58	12.3	122.0
Borneo 94	D24_BOR	Southeast Asia	Central Borneo	Turner unpublished; Scott and Irish (2017)	144	1.5	114.5
Australia—North BP	D25_AUN	Australia	Northeast Australia	Turner unpublished; Scott and Irish (2017)	57	−20.8	139.5
New Britain 1_4 738 BP_ no 3	D26_NBR	Melanesia	New Britain	Turner unpublished; Scott and Irish (2017)	238	−6.0	150.0
Nepal 94 BP	D27_NEP	South Asia	Central Nepal	Turner unpublished	97	28.0	84.0
Greek recent	D28_GRK	South Europe	South Greece	Irish et al. (2017)	70	37.5	22.3
Italy modern	D29_ITY	South Europe	Central Italy	Irish et al. (2017)	55	42.0	14.0
Kaberla 1,2,3 (13–17th century)[c]	D30_KBR	North Europe	North Estonia	Turner unpublished	160	59.5	25.3
Ladoga Finns	D31_FIN	North Europe	Finland/Western Russia	Turner unpublished	51	61.0	30.0
Lapps (Kola Peninsula)	D32_LAP	North Europe	Lapland/Northwest Russia	Turner unpublished; Scott and Irish (2017)	64	67.0	40.0
				Total	**2169**		
				Grand Total	**2844**		

[a] Samples contain some pre–19th century specimens.
[b] Only data recorded by Irish from this article were used in the present study.
[c] Sample specimens are all pre–19th century.

Table 2
The 32 recent genetic samples from Irish et al. (2020) used in the present study with background information.

Sample name	Abbreviation	Region	Country/area	Data source	*n*	Lat	Lon
Africa							
Moroccan	G1_MOR	North Africa	Morocco, Casablanca	Lazaridis et al. (2014)	10	33.5	−7.6
Algerian	G2_ALG	North Africa	Algeria	Lazaridis et al. (2014)	7	36.8	3.0
Kikuyu	G3_KKU	East Africa	Kenya	Lazaridis et al. (2014)	4	−0.4	36.9
Khomani (San)	G4_KHO	South Africa	South Africa	Lazaridis et al. (2014)	11	−27.8	21.1
Ju_hoan_North (San)	G5_JUH	South Africa	Namibia	Patterson et al., (2012); Pickrell et al., (2012)	21	−18.9	21.5
Wolof	G6_WOL	West Africa	Gambia	Gambian Genome Variation Project	5	13.4	−16.7
Mozabite	G7_MOZ	North Africa	Algeria	Patterson et al. (2012)	21	32.0	3.0
Somalia	G8_SOM	East Africa	Somalia	Lazaridis et al. (2014)	13	5.6	48.3
Sotho	G9_SOT	South Africa	South Africa	Patterson et al. (2012)	1	−29.0	29.0
Tswana	G10_TSW	South Africa	South Africa/Botswana/ Namibia	Patterson et al., (2012); Pickrell et al., (2012)	7	−28.0	24.0
Yoruba	G11_YOR	West Africa	Nigeria	Lazaridis et al. (2014)	70	7.4	3.9
Zulu	G12_ZUL	South Africa	South Africa	Patterson et al. (2012)	1	−28.0	31.0
				Total	**171**		
America, Asia, Australia, Melanesia, Europe							
Pima	G13_PIM	Mesoamerica	Chihuahua, Mexico	Patterson et al. (2012)	14	29.0	−108.0
Aleut (Nikolskoye)	G14_ALE	East Russia	Bering Island, Russia	Lazaridis et al. (2014)	2	55.2	166.0
Kyrgyz	G15_KRG	Central Asia	North Kyrgyzstan	Lazaridis et al. (2014)	9	42.9	74.6
Mongola	G16_MON	Central Asia	East Mongolia	Patterson et al. (2012)	6	45.0	111.0
Mansi	G17_MAN	Central Asia	Central Russia (Konda River)	Lazaridis et al. (2014)	3	62.5	63.3
Chukchi	G18_CHU	Central Asia	Northeast Russia	Lazaridis et al. (2014)	10	69.5	168.8
Thai	G19_THA	East Asia	Central Thailand	Lazaridis et al. (2014)	10	13.8	100.5
Kinh_Vietnam_KHV	G20_KIN	East Asia	North Vietnam	Lazaridis et al. (2014)	8	21.0	105.9
Japanese	G21_JAP	East Asia	Central Japan	Patterson et al. (2012)	29	38.0	138.0
Malays	G22_MAL	Southeast Asia	Central Malaysia	Skoglund et al. (2016)	9	4.2	102.0
Visayan, Kankanaey, Ilocano, Tagalog	G23_PHI	Southeast Asia	Central Philippines	Skoglund et al. (2016)	21	9.8	125.5
Lebbo	G24_LEB	Southeast Asia	Central Borneo	Skoglund et al., (2016) (signed letter)	8	0.0	115.0
CAI - North Australia/Queensland, WPA—North Australia/ Queensland, Australian_ECCAC	G25_AUN	Australia	Northeast Australia	Lazaridis et al. (2014)	3	−16.9	145.0
All HO New Britain from Skoglund et al. (2016)	G26_NBR	Melanesia	New Britain	Skoglund et al., (2016) (signed letter)	156	−5.8	150.8
Kusunda	G27_KUS	South Asia	Central Nepal	Lazaridis et al. (2014)	10	28.1	82.5
Greek_Coriell	G28_GRK	South Europe	East Greece	Lazaridis et al. (2014)	20	38.0	23.7
Italian_Tuscan	G29_ITY	South Europe	Central Italy	Patterson et al. (2012)	20	43.0	11.0
Estonian	G30_EST	North Europe	West Estonia	Lazaridis et al. (2014)	10	58.5	24.9
Finnish_FIN	G31_FIN	North Europe	South Finland	Lazaridis et al. (2014)	8	60.2	24.9
Saami_WGA	G32_SAM	North Europe	North Finland	Lazaridis et al., (2014); Mallick et al., 2016	3	68.4	23.6
				Total	**359**		
				Grand Total	**530**		

Melanesia, and the Americas (see Fig. 1) are described in these tables as well. Each is abbreviated with a prefix of 'D' (dental) or 'G' (genetic), followed by 1–32 and several letters. For example, Bedouin dental sample D1_BED (Table 1) is paired with genetic sample G1_MOR from Morocco (Table 2).

Matches were based on shared language, ethnic group (Turner, 1985; Irish, 1993, 1997, 2000, 2016; Irish et al., 2014; Scott et al., 2018), and geographic location. An exception to the latter criterion is the >1360-km distance between dental and genetic samples from the Russian and American sides of the Aleutians. They and the two matched Pima samples, separated by 582 km, were included to provide at least some New World coverage. Ample Native North American dental data exist (Scott et al., 2018) but corresponding genetic data do not (Reich et al., 2012; Skoglund et al., 2015); the opposite is true for these datasets in Mesoamerica and South America.

We then matched five 'ancient' dental (n = 323 individuals) and genetic (n = 36) samples by East or South African origin and period: Early, Middle, or Late Holocene (Table 3). Each is labeled with a 'D' or a 'G,' followed by an 'a' (ancient), and more letters, e.g., East Africa Middle Holocene dental sample Da_EHM is matched with genetic sample Ga_EHM. Beyond South Africa Middle Ga_SHM and Early Holocene Ga_SHE, all samples comprise individuals from multiple locales. For these, we provided mean latitude and longitude of origin sites. SNP data from the recently studied genetic sample from Mota, Ethiopia (Lipson et al., 2022), were also included. As stated, given the current, limited availability and uneven geographic and temporal distribution of ancient genomic data in Africa, these samples are used here to assess concordance with phenetic patterns rather than serve as a primary basis for reconstructing population history.

2.2. Dental data and distance analyses

The advantages and justification of using ASUDAS traits are detailed elsewhere (Turner et al., 1991; Scott and Irish, 2017; Scott et al., 2018). In brief, aside from an important genetic input, these traits have little or no sexual dimorphism—to promote sample pooling; remain observable despite some crown wear; and are evolutionarily conservative for diachronic comparisons. All 25 were used in African studies by the first author ([J.D.I.] [references in Irish et al., 2020; Irish and Usai, 2021]), including the present African samples. They are also used in the dataset of CG Turner II (Scott et al., 2018), including all non-African samples from Table 1. Recording involves referencing standardized rank-scale expressions to minimize observer error. For the trait list, refer to SOM Tables S1 and S2.

Table 3
Ancient dental and genomic African samples analyzed in the study with background information.

	Abbreviation	Country	Locations	~Date BP[a]	Data source	*n*	Lat	Lon
Dental Sample								
East Africa Middle Holocene	Da_EHM	Kenya	Homa, Hyrax Hill, Makalia, Njoro, Nakuru, Willey's Kopje[b]	3450–2950	Irish unpublished	69	0.3	36.3
East Africa Early Holocene	Da_EHE	Kenya	Bromhead's Site, Gambles Cave II, Lothagam[b]	10,000–5950	Irish unpublished	80	1.4	36.4
South Africa Late Holocene	Da_SHL	South Africa	Coburn, Gordon's Bay, Hout, Bay, Humansdorp, Melkbosstrand, Kommetjie, Llandudno, Robberg, Saldanha	2000–200	Irish et al., (2014) [c], Irish unpublished	92	−32.7	18.4
South Africa Middle Holocene	Da_SHM	South Africa	Buffel's Bay, Great Brak, Plettenberg Bay, Robberg Cave	3800–2100	Irish et al., (2014) [c]	42	−33.9	19.6
South Africa Early Holocene	Da_SHE	South Africa	Elands Bay, Fish Hoek, Knysna, Oakhurst Rockshelter, Still Bay	12,000–4100	Irish et al., (2014) [c]	40	−33.6	23.4
					Total	**323**		
Genomic Sample								
East Africa Middle Holocene	Ga_EHM	Kenya	Hyrax Hill, Kakapel, Lukenya, Nakuru, Nyanrindi, Prette John's Gully	3670–2310	Prendergast et al. (2019); Wang et al., (2020)	18	−0.46	36.0
East Africa Early Holocene	Ga_EHE	Kenya/Tanzania	Victoria Nyanza/Dodoma Kondoa	6200–4400	Prendergast et al. (2019); Lipson et al., (2022)	3	−1.8	34.8
South Africa Late Holocene	Ga_SHL	South Africa	Balito Bay, Faraoskop Rock Shelter, Kasteelberg, Oakhurst Rockshelter	2000–1180	Skoglund et al., (2017), Schlebusch et al., (2017), Gretzinger et al., (2024)	5	−32.4	18.2
South Africa Middle Holocene	Ga_SHM	South Africa	St. Helena	2245	Skoglund et al. (2017)	1	−32.8	18.1
South Africa Early Holocene	Ga_SHE	South Africa	Oakhurst Rockshelter	10,200–4600	Gretzinger et al. (2024)	8	−33.9	22.6
Mota	Ga_Mota	Ethiopia	Gamo Highlands, Mota Cave	4000	Lipson et al. (2022)	1	6.79	38.21
					Total	**36**		

[a] Approximate dates in years before present (BP).
[b] Site information available in Leakey (1970).
[c] Only data recorded by Irish from this article were used in the present study.

Like Irish et al. (2020), we chose the MMD as most appropriate for our data and research strategy. Other methods are available, e.g., nonmetric Mahalanobis D^2 (Konigsberg, 1990), but the MMD has relevant advantages. First, calculations are based on trait frequencies, so Turner's published (Turner, 1990a; also Scott and Irish, 2017) and unpublished summary data could be compared against individual traits recorded by J.D.I. in African and other samples. Second, a bias correction for small samples is incorporated for unbiased estimates of population divergence. Third, unlike D^2, the MMD has a significance test (Sjøvold, 1973, 1977; Irish, 2010; Nikita, 2015). Finally, MMD values were shown to be more highly correlated with geographic distances (Schillaci et al., 2009; Irish, 2010, 2016). Our prior analyses of the matched dental and genetic samples further demonstrated strong correspondence between MMD and F_{ST} distances at both regional and global scales to support the use of ASUDAS-derived phenetic distances for investigating large-scale population structure.

As required for the MMD (and D^2), we dichotomized those ASUDAS traits recorded on an ordinal scale as present or absent (SOM Table S1 and S2) relative to appraised morphological thresholds (Scott and Irish, 2017). Phenetic affinities were calculated between samples, with higher values indicating greater dissimilarity. The formula corrects for low ($\leq$0.05) and high ($\geq$0.95) frequencies, and small samples ($n < 10$) (Green and Suchey, 1976; Sjøvold, 1977). Regarding the significance test, distances were compared with their standard deviations for a null hypothesis of Population 1 = Population 2 at a 0.05 alpha (Irish, 2010; Sołtysiak, 2011). We focused on magnitudes of intersample distances to consider overall global patterning, like with F_{ST} (mentioned later), but did significance testing on ancient and recent African samples. Affinities were visualized with three-dimensional metric (i.e., interval-level) multidimensional scaling (MDS) using IBM SPSS Statistics 29.0 (IBM Corp., Armonk, NY, USA). This widely used method illustrates relationships among populations from intersample distance matrices and is especially effective for identifying spatial and/or temporal gradients in such data (see Kruskal and Wish, 1978; Irish, 2010; Ponce de León et al., 2018).

2.3. Genetic data and distance analyses

Comparative SNP data from the recent samples (Table 2), except for whole-genome sequences of the western African Wolof sample, were genotyped with the Affymetrix Axiom Genome-Wide Human Origins 1 Array (AHOA) (Affymetrix Inc., Santa Clara, CA, USA; Patterson et al., 2012; Pickrell et al., 2012, 2014; Lazaridis et al., 2014; Skoglund et al., 2016, or by letters of request to these authors). Publicly available AHOA data were downloaded from the Allen Ancient DNA Resource v54.1 (dataverse.harvard.edu/dataverse/reich_lab; Mallick et al., 2024). Five low-coverage Wolof sequences (9×) from the Gambian Genome Variation Project were merged with AHOA data following our previous study (Irish et al., 2020).

Ancient African genomes (Table 3) were produced from shotgun sequencing or genotyped on a 1.2M SNP array (Mathieson et al., 2015). To reduce genotype-calling biases associated with low-coverage sequences, all genomes are pseudohaploid, where at each genotype position one allele was drawn randomly. Most ancient genomes were treated with uracil-DNA glycosylase (UDG) to remove the 5′ C-to-T and 3′ G-to-A transitions from postmortem damage (Briggs et al., 2010). CpG-context transition sites, which are not repaired by UDG treatment due to methylation, were also removed. Lastly, transition sites were removed from the two Ga_SHL ancient genomes that did not undergo UDG treatment.

We used F_{ST} as a measure of genetic differentiation between populations. Our rationale for choosing it is detailed in Irish et al. (2020). In brief, it 1) excels in handling small samples, particularly when many loci are included, 2) gives reliable results on a broad

geographic scale, 3) is not directly constrained by population divergence time, and 4) provides pairwise values that remain unchanged if samples are added or removed during analyses, like the MMD. F_{ST} was calculated with POPSTATS (Skoglund et al., 2015) to yield generalized estimates of intersample genetic differentiation for comparison with MMD distances. It has no significance test. Our intention, simply, was to facilitate the interpretation of among-sample variation relative to known and hypothesized population structure and history (Relethford and Harpending, 1994). Finally, to further improve the accuracy of distances from genomic data, particularly those of very small sample size (Bhatia et al., 2013; Ortega-Del Vecchyo and Slatkin, 2019), we used the Hudson F_{ST} estimator (Hudson et al., 1992). Pairwise values were visualized with MDS. Again, these results are primarily used to evaluate the extent to which phenetic patterns derived from ASUDAS traits are consistent with genomic patterning, not as an independent basis for inference.

2.4. Minimum-slope geographic distances

We calculated geographic distances among sets of dental and genetic samples from site latitudes and longitudes (Tables 1–3). Again, global great-circle distances could be compared with MMD and F_{ST}, but topographic barriers (mountains, seas, or oceans) mean they are neither appropriate nor realistic. So, alternative approaches have been devised. Ramachandran et al. (2005) used global 'way points' with straight-line distances to avoid open water, though these had to be predefined. In a similar vein, Manica et al. (2005) identified the shortest routes between sites on land surfaces only, alongside paleoclimate data. Their method was modified by Betti et al. (2009) with graph theory to model movement on land, skirting mountains >2000 m high.

Here, we determined the most efficient routes across topography—minimum cumulative slope paths—that reduce the amount of surface slope traversed and therefore avoid major topographic barriers. We did this by using least cost path analysis on a 'cost surface' represented by the surface slope of a digital elevation model in QGIS v3.40.2 (qgis.org/). This approach means that potential paths across steep topography have a high cost to traverse (i.e., steep potential paths are penalized) while implicitly including distance due to the cumulative nature of the approach. The final route is determined as the potential path between the origin and endpoint with the minimum cumulative cost.

This strategy differs from the methods cited earlier in that it does not require predefined waypoints beyond the origin and end locations, directly incorporates topography, and avoids arbitrary elevation thresholds or additional paleoclimate inputs. Our minimum cumulative slope path approach is also entirely agnostic to any dispersal routes previously noted in the literature, with routes defined solely by topography.

The slope cost surface was generated in Google Earth Engine (Gorelick et al., 2017) by initially deriving a first-order approximation of paleotopography globally at a 5-km resolution to preserve finer-scale topographic information. This approach was implemented by combining a digital elevation model of modern land above sea level (MERIT DEM; Yamazaki et al., 2017) with a bathymetric elevation map (GEBCO Compilation Group, 2024), where the final pixel value represents the lowest altitude within each 5 × 5-km region. The goal was to preserve topographic features, such as large valleys, that could represent least-cost paths. For the now-submerged topography (c.f., Bailey and Cawthra, 2023), we took a eustatic sea-level lowstand of −116 m to represent maximum sea-level equivalent held by the ice sheets during the Last Glacial Maximum (LGM) (Gowan et al., 2021). While local sea levels during the last glaciation would be dependent on time-transient local and global ice mass configurations, we did not account for local isostatic effects in deriving our topographic mask or include paleo–ice sheet extents as topographic barriers (c.f., Gowan et al., 2021). This strategy applies a minimal-assumption approach while remaining agnostic regarding the timing of the human dispersal within and out of Africa and possible routes connecting sample sites during the global expansion.

The final cost surface was determined by calculating the gradient between each 5-km pixel of the preprocessed digital elevation model, with areas of water assigned a cost value greater than the sum of all land pixel values globally. By imposing such a high-cost value to areas of sea and ocean, these cells could only be traversed as a last resort, with the path across water being the shortest possible straight line between landmasses (e.g., Island Southeast Asia).

It should be emphasized that the routes are derived from a minimal-assumption analysis of paleotopography and therefore should not necessarily be interpreted as the actual migration pathways. Similarly, where the method does not replicate suggested dispersal pathways, it does not negate their plausibility. This contrasts with prospective routes employing archaeological, paleoenvironmental, paleontological, or other empirical data—like the southern dispersal from East Africa, coastal or beachcomber model for South Asia, or a coastal migration from Beringia to the Americas (overviews in Garcea, 2010; Reyes-Centeno et al., 2017; Langgut et al., 2018; Beyer et al., 2021; Nicholson et al., 2021; Abbas et al., 2023; Bailey and Cawthra, 2023; Saltré et al., 2024).

2.5. Mantel correlations

Mantel tests, with a null hypothesis of no association between matrices, were used to calculate Pearson correlations between dental, genetic, and minimum-slope geographic distances; they are widely used in population genetics and biological anthropology to assess the correspondence between matrices from different data types (details in Smouse and Long, 1992; Sokal and Rohlf, 1995). Though not without criticism (Legendre and Fortin, 2010; Guillot and Rousset, 2013), Mantel tests have been proven methodologically robust (Séré et al., 2017), are easy to interpret, and remain widely used for comparability among studies. We submitted matrices to the Mantel test module in PAST 3.23 to yield r_m values with one-tailed p values from 9999 random permutations (Hammer et al., 2001).

2.6. Linear regression

Finally, stimulus coordinates on the first dimension of MDS plots for each sample from MMD and F_{ST} matrices were regressed against minimum-slope distances, after the method by Ponce de León et al. (2018). In their Out-of-Africa study, variation in morphometric data on principal component (PC) 1 of principal component analysis (PCA) provided insights into population history and dispersal. They obtained equivalent information with MDS dimension 1 coordinates after inputting an intersample distance matrix from these data (Ponce de León et al., 2018). Because of disparity in variable count, 25 ASUDAS traits vs. >350,000 SNPs, which would provide vastly unequal variances on PC1, we applied their MDS approach—inputting the same number of strongly correlated MMD and F_{ST} intersample distances in analyses to promote comparability.

Whether PCA or metric MDS, plotting the first dimension against the second can yield a 'horseshoe' pattern (Kruskal and Wish, 1978; Novembre and Stephens, 2008; Morton et al., 2017; Shah et al., 2024), a common outcome when ordinating clinal data, i.e., when samples are ordered spatially or temporally, reflecting

gradients associated with human dispersal (Ponce de León et al., 2018). This pattern is evident in both Figure 2 plots (and highlighted in SOM Fig. S1). While sometimes viewed as a dimension-reduction artifact (Podani and Miklós, 2002; Frichot et al., 2012), most find the interpretability unaffected, with position along the gradient remaining informative of relative among-sample relationships (Kruskal and Wish, 1978). In all present MDS plots, dimension 1 separates African from non-African samples. The latter experienced the same bottleneck leaving Africa, reducing variation and resulting in greater genetic and morphological diversity within than outside the continent (Prugnolle et al., 2005; Ramachandran et al., 2005; Li et al., 2008; Jay et al., 2013; Bergström et al., 2021; Fan et al., 2023).

We calculated coefficients of determination (R^2), along with correlations (r) and p values, for all recent and ancient dental samples, followed by the same for their comparative genetic counterparts. Regional regressions (South vs. East Africa, Asia, Americas) identified samples having the highest R^2 value. With these horseshoe-like, i.e., clinal, configurations, each R^2 value and residual distribution informs (per Ponce de León et al., 2018:5) on the 'orientation of the main dispersal axis,' and the origin and farthest extent of geographic dispersal. Of course, the present population locations do not inevitably signal those of their ancestors as migrations and demographic shifts might have altered their distribution, as discussed later.

3. Results

3.1. Distance analyses

Percentages of the 25 ASUDAS traits in the 12 recent African and 20 non-African samples from Irish et al. (2020) are listed in SOM Tables S1 and S2. To promote pairing with as many genetic samples for concordance purposes as possible, some sample observations were smaller than the MMD formula is designed to correct for ($n < 10$). These few exceptions warrant attention, but the MMD is a robust statistic, so results should not be substantially affected (Irish, 2010). The matrix is presented in SOM Table S3, from which the MDS graph in Figure 2A (given earlier) was derived. With a Kruskal's stress value of 0.09 and an R^2 value of 0.96, this solution is a good fit of the data (Dugard et al., 2022). To assess concordance with patterns yielded by these analyses, F_{ST} distances from SNP data in the 32 recent African/non-African matched genetic samples were calculated and are listed in SOM Table S4. This MDS solution is also a good fit (i.e., stress = 0.07, $R^2 = 0.98$). Its distribution evidences less sample variation within geographic regions (Fig. 2B), but MDS plots from both distance matrices show comparable African/non-African relationships.

We next calculated percentages for the five ancient East and South African dental samples (Table 4). An abridged MMD matrix (Table 5) and MDS plot (Fig. 3; stress = 0.08, $R^2 = 0.97$) position them near recent Sub-Saharan Africans. Da_EHM and Da_EHE do not significantly differ ($p > 0.05$) from East Africans (D3_KKU, D8_SOM; MMD ≤ 0.01) or most of the other recent Sub-Saharan samples—except the South African Bantu-speaking Zulu (D12_ZUL) and the Khoesan (D4_RRI, D5_SAN). On the other hand, Da_SHL, Da_SHM, and Da_SHE are like Khoesan (0.00–0.02), with some resemblance to the other South African 'Bantu' (D9_SOT, D10_TSW, 0.01–0.06). Otherwise, with minor shifting, the distribution parallels Figure 2A, including some proximity of Melanesian D26_NBR to Sub-Saharan Africans (also Fig. 4 below).

Conversely, an abridged F_{ST} matrix from SNP data in the five matched ancient genetic samples (Table 6) revealed that inter-sample distances of Ga_EHE, Ga_SHL, Ga_SHM, and Ga_SHE are substantially higher than in recent Sub-Saharan African ($F_{ST} = 0.24–0.55$) and other global samples. Distances of the fifth sample, Ga_EHM, are smaller (0.07–0.18) but not comparable to the MMD affinities of matched dental sample Da_EHM. The unmatched sample Ga_Mota is relatively distinct from all. The ancient genetic samples are all highly divergent from one another (F_{ST}~0.4–1.0). To demonstrate, a simple two-dimensional MDS plot was generated (SOM Fig. S2). All recent samples appear 'forced' to the center, with only Ga_EHM in the general vicinity of East Africans; other ancient samples are on the plot margins. Stress is high (0.21) to indicate a poor fit. This result is probably an artifact of the very small ancient sample sizes ($n = 1–8$), except perhaps Ga_EHM ($n = 18$), along with missing genotype data. It is likely that these

Table 4
Percentages of 25 ASUDAS traits considered present and individuals scored (n) in the five ancient East and South African samples.

Trait/Grades Present		Da_EHM[a]	Da_EHE	Da_SHL	Da_SHM	Da_SHE
Winging I^1	%	2.9	0.0	1.4	3.3	4.0
(+ = ASU 1)[b]	*n*	34	36	72	30	25
Shoveling I^1	%	0.0	0.0	5.0	0.0	11.1
(+ = ASU 3–6)	*n*	27	24	20	18	9
Double Shoveling I^1	%	0.0	0.0	0.0	0.0	0.0
(+ = ASU 2–6)	*n*	28	26	36	25	13
Interruption Groove I^2	%	3.6	6.9	3.6	0.0	0.0
(+ = ASU +)	*n*	28	29	28	14	10
Tuberculum Dentale I^2	%	28.6	34.5	27.3	7.7	22.2
(+ = ASU 2–6)	*n*	28	29	22	13	9
Bushman Canine UC	%	3.7	9.4	41.2	40.0	55.6
(+ = ASU 1–3)	*n*	27	32	17	15	9
Hypocone M^2	%	68.1	73.8	96.8	93.8	91.7
(+ = ASU 3–5)	*n*	47	42	63	32	24
Cusp 5 M^1	%	8.0	16.7	23.3	31.6	28.6
(+ = ASU 2–5)	*n*	25	36	30	19	14
Carabelli's trait M^1	%	38.5	34.2	26.7	15.8	18.2
(+ = ASU 3–7)	*n*	26	38	30	19	11
Parastyle M^3	%	0.0	0.0	0.0	0.0	0.0
(+ = ASU 3–5)	*n*	46	39	48	18	18
Enamel Extension M^1	%	0.0	3.6	0.0	2.8	0.0
(+ = ASU 1–3)	*n*	20	28	60	36	26
Root Number P^1	%	63.3	75.0	49.3	33.3	33.3
(+ = ASU 2+)	*n*	30	12	69	30	27
Root Number M^2	%	68.0	75.0	78.6	66.7	79.0
(+ = ASU 3+)	*n*	25	20	42	18	19
Odontome P1–P2	%	0.0	0.0	1.64	0.0	0.0
(+ = ASU +)	*n*	60	51	61	26	21
Congenital Absence M^3	%	1.7	0.0	4.8	11.4	6.5
(+ = ASU −)	*n*	58	53	84	35	31
Lingual Cusp P_2	%	59.3	64.9	82.9	80.0	92.9
(+ = ASU 2–9)	*n*	54	37	41	15	14
Groove Pattern M_2	%	62.3	65.6	72.3	82.8	59.1
(+ = ASU Y)	*n*	61	61	65	29	22
Cusp Number M_1	%	4.8	3.8	4.7	8.3	0.0
(+ = ASU 6+)	*n*	42	53	43	24	13
Cusp Number M_2	%	66.1	78.9	96.3	100	100
(+ = ASU 5+)	*n*	56	52	54	27	17
Protostylid M_1	%	0.0	0.0	0.0	0.0	9.1
(+ = ASU 3–6)	*n*	42	55	24	20	11
Cusp 7 M_1	%	21.4	23.3	16.4	34.6	30.0
(+ = ASU 2–4)	*n*	42	60	55	26	20
Tome's root P_1	%	19.1	15.0	12.3	4.2	23.5
(+ = ASU 3–5)	*n*	21	20	65	24	17
Root Number LC	%	2.5	2.9	0.0	0.0	0.0
(+ = ASU 2+)	*n*	40	35	66	26	21
Root Number M_1	%	3.1	0.0	0.0	0.0	0.0
(+ = ASU 3+)	*n*	32	28	49	16	14
Root Number M_2	%	89.7	95.5	88.7	90.0	71.4
(+ = ASU 2+)	*n*	29	22	53	20	14

ASUDAS = Arizona State University Dental Anthropology System.
[a] Da_EHM = East African Middle Holocene, Da_EHE = East African Early Holocene, Da_SHL = South African Late Holocene, Da_SHM = South African Middle Holocene, Da_SHE = South African Early Holocene. Details are mentioned in Table 3 of the main text.
[b] ASUDAS rank-scale trait breakpoint information in Irish (1993, 1997, 2005, 2006), Scott and Irish (2017) and Scott et al. (2018).

Table 5
Mean measure of divergence distance matrix for the five ancient East and South African dental samples based on 25 ASUDAS traits, plus pooled East and South African samples (Da_EHol, Da_SHol).[a]

Sample	Da_EHM	Da_EHE	Da_SHL	Da_SHM	Da_SHE	Da_EHol	Da_SHol
D1_BED	0.047[b]	0.078	0.218	0.262	0.282	0.076	0.258
D2_KAB	0.044	0.074	0.236	0.310	0.298	0.076	0.288
D3_KKU	0.008	0.000	0.024	0.060	0.082	0.008	0.076
D4_RRI	0.074	0.048	0.000	0.000	0.000	0.072	0.000
D5_SAN	0.095	0.061	0.015	0.022	0.004	0.089	0.030
D6_SEN	0.000	0.000	0.097	0.152	0.124	0.005	0.151
D7_SHA	0.098	0.117	0.231	0.285	0.278	0.125	0.273
D8_SOM	0.000	0.000	0.121	0.157	0.173	0.002	0.171
D9_SOT	0.023	0.000	0.011	0.030	0.059	0.017	0.057
D10_TSW	0.015	0.003	0.017	0.006	0.038	0.019	0.043
D11_YOR	0.003	0.000	0.057	0.130	0.083	0.006	0.124
D12_ZUL	0.039	0.010	0.033	0.046	0.062	0.035	0.079
D13_PIM	0.558	0.595	0.645	0.680	0.602	0.604	0.692
D14_ALE	0.475	0.542	0.624	0.596	0.572	0.526	0.644
D15_KAZ	0.259	0.330	0.403	0.422	0.373	0.309	0.427
D16_MON	0.533	0.584	0.622	0.610	0.526	0.579	0.641
D17_LOK	0.361	0.417	0.487	0.488	0.422	0.408	0.500
D18_CHU	0.559	0.634	0.730	0.717	0.687	0.615	0.764
D19_THA	0.374	0.398	0.392	0.412	0.337	0.403	0.425
D20_VIE	0.348	0.378	0.431	0.443	0.383	0.383	0.469
D21_JAP	0.476	0.519	0.539	0.544	0.467	0.522	0.577
D22_MAL	0.194	0.188	0.252	0.294	0.254	0.210	0.301
D23_PHI	0.318	0.339	0.411	0.447	0.369	0.349	0.454
D24_BOR	0.290	0.308	0.333	0.361	0.279	0.321	0.377
D25_AUN	0.349	0.332	0.335	0.322	0.330	0.356	0.346
D26_NBR	0.189	0.185	0.237	0.264	0.282	0.200	0.267
D27_NEP	0.283	0.353	0.457	0.458	0.425	0.334	0.491
D28_GRK	0.040	0.063	0.206	0.233	0.250	0.064	0.253
D29_ITY	0.080	0.099	0.278	0.358	0.360	0.101	0.343
D30_KBR	0.141	0.189	0.322	0.367	0.350	0.181	0.364
D31_FIN	0.181	0.239	0.416	0.481	0.464	0.227	0.476
D32_LAP	0.305	0.355	0.456	0.468	0.423	0.348	0.465
Da_EHM	0.000	0.000	0.077	0.107	0.122		
Da_EHE	0.000	0.000	0.039	0.076	0.095		
Da_SHL	0.077	0.039	0.000	0.000	0.000		
Da_SHM	0.107	0.076	0.000	0.000	0.000		
Da_SHE	0.122	0.095	0.000	0.000	0.000		
Da_EHol						0.000	0.115
Da_SHol						0.115	0.000

ASUDAS = Arizona State University Dental Anthropology System.
[a] Da_EHol = East African Holocene pooled (Da_EHM, Da_EHE), Da_SHol = South African Holocene pooled (Da_SHL, Da_SHM, Da_SHE), for comparison with pooled genomic samples. See text.
[b] Underlined values indicate significant difference between sample pairs at $p \leq 0.05$.

high values do not reliably quantify population diversity, so to assess the validity of our ancient dental data and results as desired, pooling was conducted to maximize genetic sample sizes.

Mean measure of divergence distances for pooled ancient dental samples Da_EHol ($n = 149$) and Da_Shol ($n = 174$), from the two East and three South African Holocene samples (Table 3), are also listed in Table 5. This MDS solution (Fig. 4A; stress = 0.08, $R^2 = 0.97$) visualizes intra-regional and inter-regional relationships comparable to the preceding dental plots. Da_EHol shows a close affinity to the East Africans (MMD = 0.00–0.01, $p > 0.05$) and most other recent Sub-Saharan Africans; again, differences from the Zulu and Khoesan samples are significant. Da_Shol is akin to Khoesan (0.00–0.03) but differs from the other two South African Bantu-speaking groups.

Ga_EHol ($n = 21$) and Ga_SHol ($n = 14$) were assembled from the two East and three South African Holocene samples (Table 3). Genetically and geographically distinctive Ga_Mota ($n = 1$) from northern Ethiopia was dropped from further analyses. Pooled intersample F_{ST} distances became smaller (Table 6), showing that small sample size was a fundamental reason for the drift observed between ancient and recent samples (SOM Fig. S2). Yet, unlike the dental results, these genetic samples are at some distance from recent Sub-Saharan Africans in Figure 4B (stress = 0.07, $R^2 = 0.98$).

3.2. Minimum-slope geographic distances

The matrix of minimum-slope distances among sites for the 32 recent dental samples is provided in SOM Table S5, with those for the five ancient and two pooled dental samples in SOM Table S6. Figure 5A identifies paths among recent and ancient dental samples, with elevation and LGM vs. modern coastlines indicated. Equivalent minimum-slope distances among the 32 recent and five ancient genetic samples (plus Mota) were calculated but are not presented; those among recent and pooled ancient samples are listed in SOM Table S7. Their locations and paths are illustrated in Figure 5B.

3.3. Mantel tests

Correlations between the MMD and minimum-slope geographic matrices for all combinations of recent and ancient dental sample comparisons are strongly positive and significant ($r_m > 0.70$; see Table 7). That between F_{ST} and minimum slope for the recent genetic samples is equally strong. However, due to the extreme F_{ST} distances (mentioned earlier), the correlation between the matrix of ancient African and recent samples with minimum slope is very weak. Pooling the ancient samples to represent East vs. South Africa improved results. Combined with recent samples, their F_{ST} matrix provided a significant correlation >0.60 with minimum slope.

Finally, the correlation between MMD and F_{ST} distances for the recent dental and genetic samples is >0.70. That between the matched sets of recent and five ancient samples is weak and insignificant, while the correlation between MMD and F_{ST} from matched recent/ancient pooled samples reached ≤0.70. Because of the criterion for geographic proximity in matching dental and genetic samples, correlations between matrices from the three sets of minimum-slope distances are all >0.98 and significant.

3.4. Regression analyses

The range of coefficients of determination (R^2) for the recent Sub-Saharan African dental samples is 0.56–0.75 (r = 0.75–0.86), as listed in Table 8. Reflecting their greater dental diversity, the highest values are associated with South African Khoesan (D4_RRI and D5_SAN), as well as Bantu-speaking groups (D9_SOT, D10_TSW, and D12_ZUL); they are then lower in East (D3_KKU and D8_SOM) and lowest in West Africans (D6_SEN and D11_YOR). In North Africa, the range is 0.49–0.55 (D1_BED, D2_KAB, and D7_SHA). For all results, the p value is <0.01. Outside the continent, R^2 values drop suddenly in Europe (~0.00–0.04, $p = 0.26$–0.80) and parts of Central (0.03–0.07, $p = 0.14$–0.36) and South Asia (~0.00, $p = 0.82$). A slight uptick occurs in Southeast Asia (0.14–0.18, $p = 0.02$–0.03) and, to a lesser extent, in Melanesia and Australia (~0.11, $p = 0.06$–0.07). An increase is then indicated in East Asians (0.20–0.46) and, unsurprisingly (c.f., Ponce de León et al., 2018), in the geographically most distant northern Siberia (0.65–0.76) and Americas (D13_PIM, 0.79; D14_ALE, 0.81), with all R^2 values significant ($p < 0.01$). Exemplar plots for the samples from South Africa (D4_RRI), Greece (D28_GRK), and the Aleutian Islands (D14_ALE) are supplied (Fig. 6A–C).

In the 32 matched recent genetic samples, R^2 values (Table 9) mirror the dental results: 0.59–0.83 (r = 0.77–0.91, $p < 0.01$). Indicating greater genetic diversity, the highest R^2 value resulted from Khoesan (G4_KHO and G5_JHN) and 'Bantu' samples

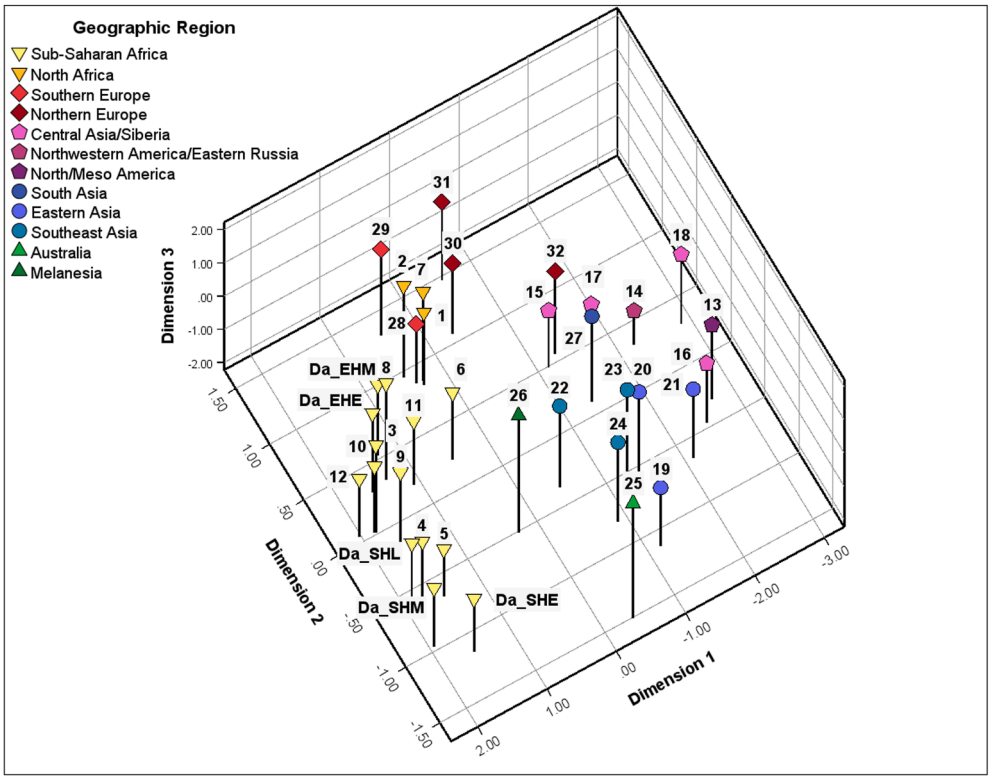

Figure 3. Multidimensional scaling plot of MMD distances among 32 recent global and five ancient Sub-Saharan African dental samples. Numbers refer to sample abbreviations in Table 1. Da_EHM = East African Middle Holocene, Da_EHE = East African Early Holocene, Da_SHL = South African Late Holocene, Da_SHM = South African Middle Holocene, Da_SHE = South African Early Holocene. Details are mentioned in Table 3 and in text. MMD = mean measure of divergence. (For interpretation of the references to color in this figure, the reader is referred to the web version of this article.)

(G9_SOT, G10_TSW, and G12_ZUL); the pairwise F_{ST} distances among these samples (SOM Table S3) are also ~0.00. R^2 values are slightly lower in East (G3_KKU and G8_SOM) and, more so, in West Africa (G6_WOL and G11_YOR). North Africans are 0.49–0.57. For all results, the p value is <0.01. They again drop in Europe ($R^2 = 0.01–0.05$, $p = 0.24–0.60$) and in areas of Central (0.01–0.05, $p = 0.20–0.57$) and South Asia (0.03, $p = 0.35$). Succeedingly higher R^2 values then result in Southeast Asia (0.29–0.31), Melanesia/Australia (~0.29), East Asia (0.29–0.39), northern Siberia (0.53–0.60)—which includes Russian Aleuts (G14_ALE; $R^2 = 0.64$, $p < 0.01$)—and the Americas (G13_PIM); for all results, the p value is <0.01. Regression plots (Fig. 6D–F) were rendered for the South Africa (G4_KHO), Greece (G28_GRK), and Aleutian (G14_ALE) samples.

Regressing dimension 1 coordinates (Fig. 3) against minimum-slope distances for the 32 recent and five ancient Sub-Saharan dental samples, Da_EHM, Da_EHE, Da_SHL, Da_SHM, and Da_SHE, increased the R^2 value for all recent samples by 0.03 on average (Table 8). So, the trends of intersample variation remain largely constant (compare Figs. 2a and 3). Significant R^2 values are high for ancient East African Da_EHM (0.72) and Da_EHE (0.69) (r = 0.85, 0.83) and higher for the South African Da_SHL, Da_SHM, and Da_SHE (0.79, r = 0.89). For side-by-side comparisons, regression plots of Middle and Early Holocene samples by region are presented in Figure 7. Given sampling limitations, analyses were not conducted for Ga_EHM, Ga_EHE, Ga_SHL, Ga_SHM, and Ga_SHE.

Lastly, linear regressions were performed on pooled ancient dental samples Da_EHol and Da_SHol (Table 8); this afforded another comparison of R^2 values with genetic samples Ga_EHol and Ga_SHol. Their inclusion increased the R^2 value overall but not to the extent of the individual ancient samples. So again, the sample distribution is largely unchanged (compare Figs. 2A, 3, and 4A). Da_EHol and Da_SHol coefficients of determination are both high, 0.71 and 0.77 (r = 0.84, 0.88, $p < 0.01$), respectively, as seen in their regression plots (Fig. 8A, B).

The differences in R^2 values are larger between Ga_EHol and Ga_SHol (Table 9), i.e., 0.62 and 0.78 (r = 0.78, 0.89, $p < 0.01$), respectively; their regression plots are shown in Figure 8C, D. Unlike the dental output, R^2 values for their origin (Africa) and farthest extent of dispersal (Northern Siberia/Americas) decreased markedly by an average 0.12. For intermediate global locations, R^2 values increased by 0.02 among samples. Though improved, the still-divergent F_{ST} distances (Table 6; Fig. 4B) indicate that pooling did not sufficiently address the aforementioned genotype and small sample size issues.

4. Discussion

4.1. Out of Africa

Recent samples Affinities of the 32 recent dental samples (Fig. 2A), like their comparative genetic counterparts (Fig. 2B), signal IBD—with an origin in and expansion out of Africa (SOM Tables S1–S7). Comparability of results is quantified by the strongly positive correlation between MMD and F_{ST} matrices (Table 7). Addressing our first research question, this correspondence indicates that ASUDAS-based phenetic distances broadly reflect patterns observed in genetic data, consistent with their use to investigate large-scale population structure (c.f., Irish et al., 2020). Mantel correlations are equally strong between the MMD and F_{ST} matrices and their minimum-slope geographic distances. They align with remnants of Out-of-Africa II, ~70,000 to

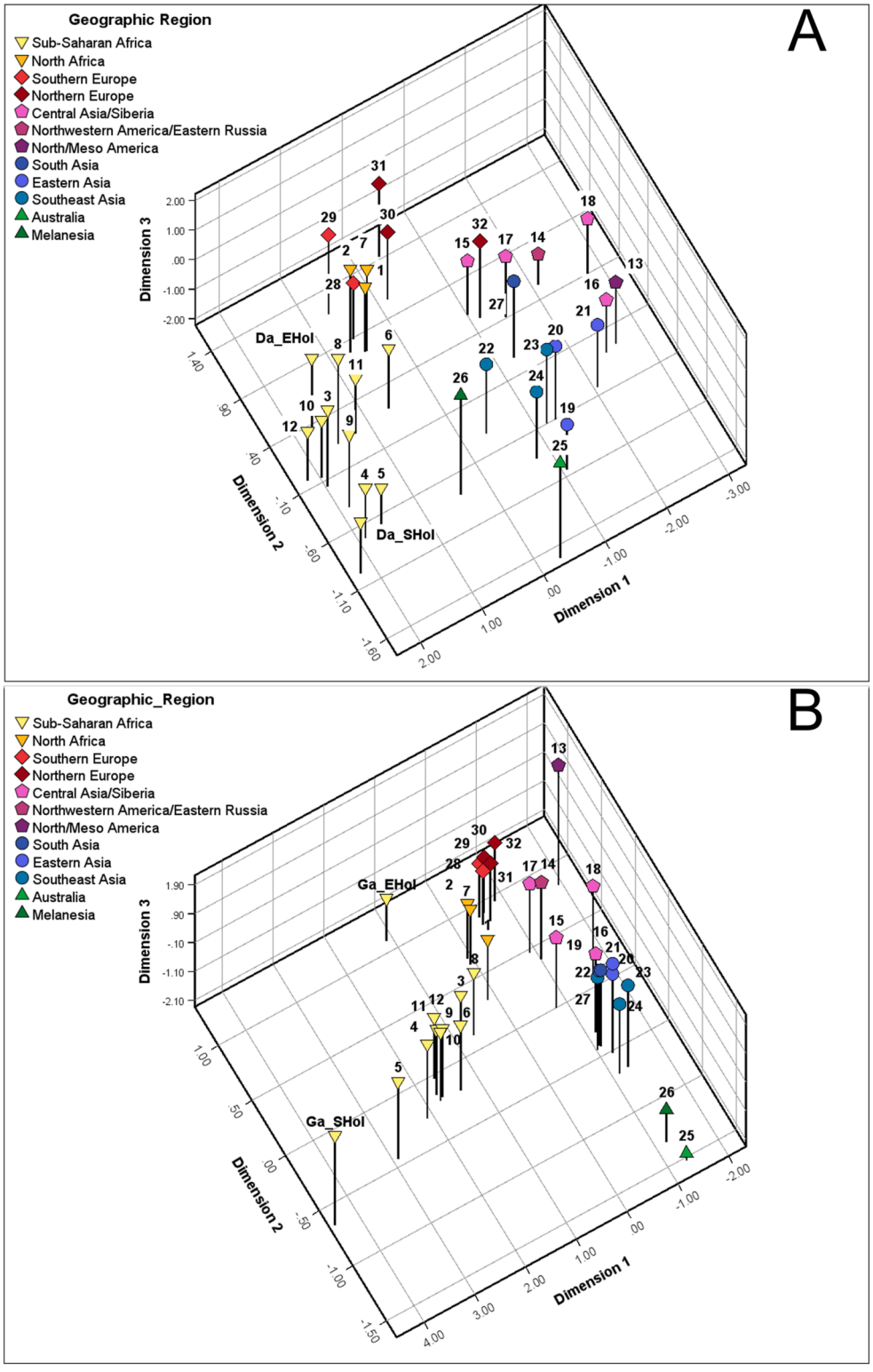

Figure 4. A) Multidimensional scaling plot of MMD distances among 32 recent global and two pooled ancient sub-Saharan African dental samples. Numbers refer to sample abbreviations in Table 1. Da_EHol = pooled East African Holocene, Da_SHol = pooled South African Holocene. See text and Table 5. B) Multidimensional scaling plot of F_{ST} distances among 32 recent global and two pooled ancient sub-Saharan African genetic samples. Ga_EHol = pooled East African Holocene, Ga_SHol = pooled South African Holocene. Numbers refer to sample abbreviations in Table 2. Details in text and Table 6. MMD = mean measure of divergence. (For interpretation of the references to color in this figure, the reader is referred to the web version of this article.)

Table 6
Hudson's F_{ST} distance matrix for the six ancient East and South African genetic samples based on single nucleotide polymorphism data, plus pooled East and South African samples (Ga_EHol, Ga_SHol).[a]

Sample	Ga_EHM	Ga_EHE	Ga_SHL	Ga_SHM	Ga_SHE	Ga_Mota	Ga_EHol	Ga_SHol
G1_MOR	0.089	0.534	0.467	0.581	0.379	0.543	0.085	0.266
G2_ALG	0.104	0.546	0.482	0.595	0.394	0.560	0.101	0.281
G3_KKU	0.077	0.491	0.419	0.533	0.320	0.504	0.068	0.203
G4_KHO	0.139	0.510	0.365	0.480	0.242	0.530	0.126	0.111
G5_JUH	0.180	0.530	0.383	0.493	0.253	0.555	0.165	0.121
G6_WOL	0.096	0.465	0.393	0.483	0.305	0.483	0.086	0.199
G7_MOZ	0.101	0.545	0.479	0.591	0.390	0.558	0.098	0.279
G8_SOM	0.070	0.507	0.439	0.552	0.347	0.516	0.064	0.229
G9_SOT	0.107	0.491	0.397	0.513	0.288	0.510	0.095	0.166
G10_TSW	0.111	0.494	0.398	0.510	0.288	0.515	0.099	0.164
G11_YOR	0.109	0.505	0.430	0.545	0.328	0.520	0.098	0.208
G12_ZUL	0.115	0.500	0.415	0.530	0.310	0.520	0.103	0.188
G13_PIM	0.247	0.663	0.598	0.706	0.509	0.679	0.241	0.400
G14_ALE	0.160	0.590	0.524	0.635	0.439	0.601	0.156	0.329
G15_KRG	0.144	0.572	0.508	0.619	0.422	0.584	0.140	0.312
G16_MON	0.172	0.591	0.529	0.638	0.441	0.603	0.168	0.333
G17_MAN	0.152	0.583	0.519	0.630	0.433	0.596	0.149	0.322
G18_CHU	0.202	0.623	0.558	0.665	0.469	0.636	0.198	0.362
G19_THA	0.169	0.589	0.524	0.633	0.439	0.603	0.164	0.330
G20_KIN	0.179	0.595	0.533	0.642	0.446	0.612	0.174	0.338
G21_JAP	0.183	0.599	0.536	0.646	0.452	0.613	0.178	0.342
G22_MAL	0.165	0.584	0.522	0.628	0.435	0.599	0.160	0.325
G23_PHI	0.187	0.607	0.541	0.650	0.454	0.619	0.182	0.345
G24_LEB	0.174	0.594	0.528	0.637	0.443	0.606	0.169	0.334
G25_AUN	0.240	0.655	0.585	0.691	0.498	0.667	0.235	0.389
G26_NBR	0.207	0.619	0.553	0.660	0.466	0.632	0.201	0.358
G27_KUS	0.171	0.593	0.530	0.639	0.442	0.604	0.166	0.331
G28_GRK	0.125	0.572	0.506	0.616	0.422	0.583	0.124	0.311
G29_ITY	0.127	0.573	0.508	0.617	0.424	0.584	0.125	0.314
G30_EST	0.136	0.580	0.513	0.627	0.428	0.590	0.134	0.318
G31_FIN	0.135	0.578	0.511	0.623	0.426	0.589	0.133	0.316
G32_SAM	0.154	0.588	0.524	0.637	0.440	0.602	0.152	0.331
Ga_EHM	0.000	0.539	0.492	0.602	0.378	0.572		
Ga_EHE	0.538	0.000	0.858	0.979	0.998	0.975		
Ga_SHL	0.486	0.863	0.000	0.855	0.431	0.889		
Ga_SHM	0.603	0.986	0.864	0.000	0.987	0.999		
Ga_SHE	0.378	0.998	0.431	0.987	0.000	0.903		
Ga_Mota	0.572	0.880	0.889	0.999	0.903	0.000		
Ga_EHol							0.000	0.255
Ga_SHol							0.255	0.000

F_{ST} = Hudson FST distance matrix.
[a] Ga_EHol = East African Holocene pooled (Ga_EHM, Ga_EHE), Ga_SHol = South African Holocene pooled (Ga_SHL, Ga_SHM, Ga_SHE), for comparison with pooled dental samples. See main text.

50,000 years ago. In general, these affinities correspond to a decline in frequencies of key Sub-Saharan mass-additive traits (Irish, 1997; mentioned later), and overall dental variation, with distance from Africa; this trend is in accord with expectations under IBD and models involving serial founder effects, as suggested by other researchers studying morphometric features (Betti et al., 2009; Ponce de León et al., 2018), genetic markers (Ramachandran et al., 2005; Jay et al., 2013; Kanitz et al., 2018; Tobler et al., 2023), and even languages (Atkinson, 2011; Pérez-Losada and Fort, 2023).

Along these lines, R^2 values are high for all recent Sub-Saharan African samples (Table 8), like their matched genetic samples (Table 9). For both, the highest are in South Africans, notably the Khoesan—the most divergent modern population with the greatest morphogenetic diversity. The high R^2 value in dental and, to a lesser degree, genetic samples from the Americas marks the farthest area of dispersal, i.e., an inverse relationship in IBD (Ramachandran et al., 2005; Ponce de León et al., 2018; see Fig. 6). For some perspective, Betti et al. (2009) obtained R^2 values $\geq$0.50 for decline of within-population craniometric diversity with distance from Africa. Ponce de León et al. (2018) reported $R^2 = 0.58$ when regressing PC1 of bony labyrinth morphology in 10 global samples against dispersal distance. To gauge the outcome, they repeated this process using F_{ST} from SNPs in 10 matched samples for $R^2 = 0.85$—like we recorded. Equivalency was reported in other genetic studies regressing F_{ST} on geographic distances, with East Africa as the dispersal origin (Prugnolle et al., 2005; Ramachandran et al., 2005; Lawson Handley and Perrin, 2007; also see Kanitz et al., 2018). That said, while these patterns are expected under serial founder models, similar clinal variation may arise under broader scenarios of spatially structured populations and long-term IBD. Accordingly, our results are interpreted as supporting, but not uniquely demonstrating, such demographic processes.

In summary of these global comparisons, genetic and phenetic distances are expected to increase with spatial and temporal separation; deviations may indicate non-neutral influences (Konigsberg, 1990; Relethford, 2004; Ramachandran et al., 2005; Duforet-Frebourg and Slatkin, 2016; Ponce de León et al., 2018). Using higher genetic-based R^2 values as a benchmark, the craniodental data performed well, aligning with neutral-like patterns at large geographic scales (Ponce de León et al., 2018; Irish et al., 2020), particularly the ASUDAS traits with Sub-Saharan samples (Table 8).

Ancient samples The inability to adequately compare the five matched ancient dental and genetic samples (Table 3), due to the

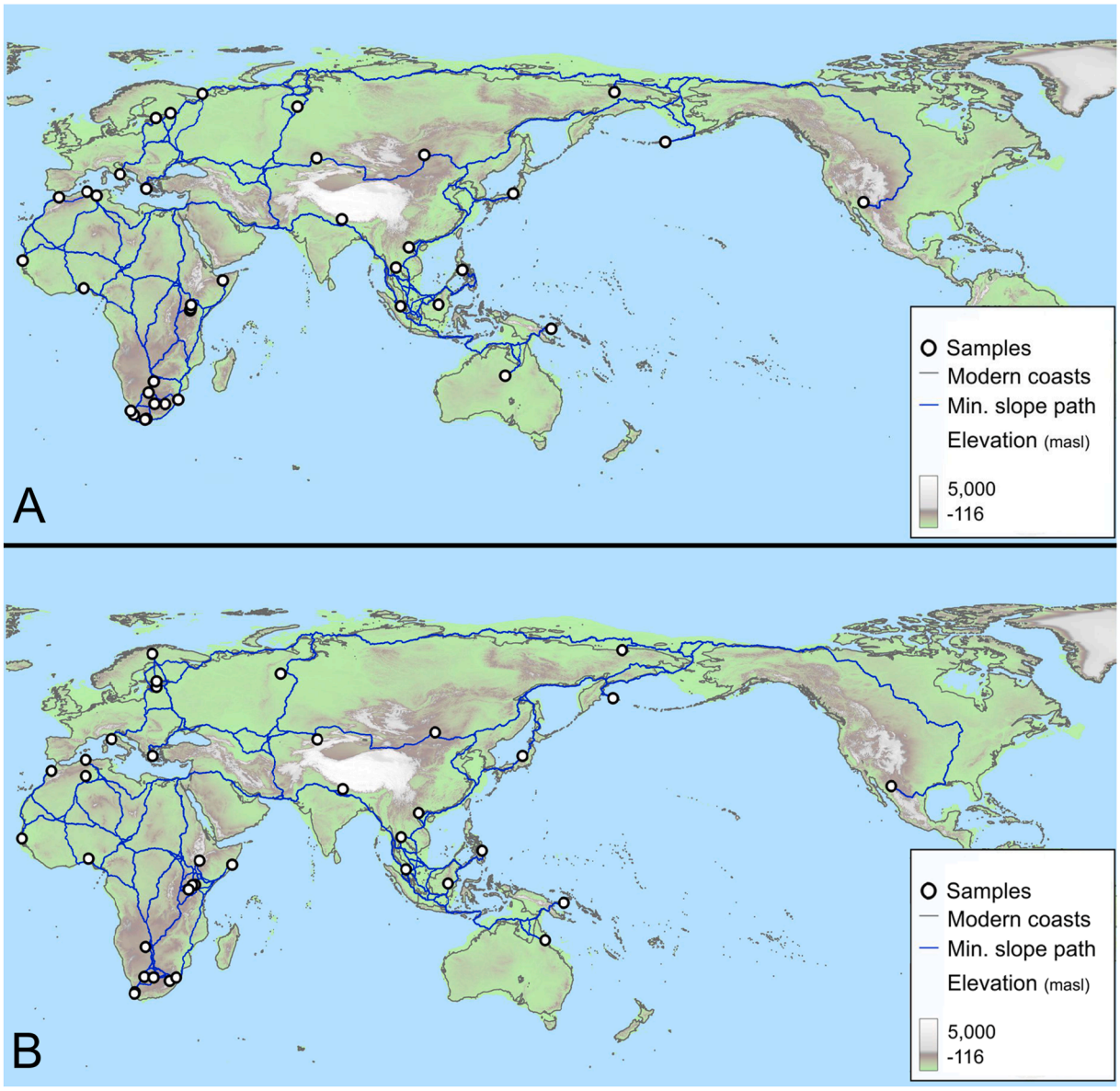

Figure 5. A) Minimum-slope geographic paths among origin sites for all recent and ancient dental samples. Details in text and SOM Tables S5 and S6. B) Minimum-slope paths among origin sites for all recent and ancient genetic samples. Details are mentioned in text and SOM Table S7. (For interpretation of the references to color in this figure, the reader is referred to the web version of this article.)

Table 7
Mantel correlation results.

Sample Analysis:		32 recent	32 recent + 5 ancient	32 recent + 2 pooled ancient
Matrices compared:				
MMD[a] and Dental Geog	r_m=	0.713	0.756	0.726
	p=	0.0001	0.0001	0.0001
F_{ST} and Genetic Geog	r_m=	0.713	0.121	0.616
	p=	0.0001	0.1233	0.0001
MMD and F_{ST}	r_m=	0.721	0.322	0.685
	p=	0.0001	0.0002	0.0001
Dental Geog and Genetic Geog	r_m=	0.988	0.990	0.989
	p=	0.0001	0.0001	0.0001

[a] MMD = mean measure of divergence matrix; Dental Geog = matrix of minimum-slope geographic distances among dental samples; F_{ST} = Hudson F_{ST} distance matrix; Genetic Geog = matrix of minimum-slope geographic distances among genetic samples. See text for details.

Table 8
Regression results for MDS dimension 1 of MMD matrix against geographic distances for the recent, recent/pooled ancient, and recent/ancient dental sample analyses,[a] listing coefficients of determination (R^2), correlations (r), and *p* values.

Analysis	Recent			Recent and ancient			Recent and pooled		
Sample	R^2	r	*p*	R^2	r	*p*	R^2	r	*p*
D1_BED	0.533	0.730	<0.001	0.542	0.736	<0.001	0.540	0.735	<0.001
D2_KAB	0.487	0.698	<0.001	0.489	0.699	<0.001	0.493	0.702	<0.001
D3_KKU	0.696	0.834	<0.001	0.726	0.852	<0.001	0.714	0.845	<0.001
D4_RRI	0.741	0.861	<0.001	0.789	0.888	<0.001	0.767	0.876	<0.001
D5_SAN	0.740	0.860	<0.001	0.785	0.886	<0.001	0.764	0.874	<0.001
D6_SEN	0.557	0.746	<0.001	0.569	0.754	<0.001	0.566	0.752	<0.001
D7_SHA	0.504	0.710	<0.001	0.508	0.713	<0.001	0.511	0.715	<0.001
D8_SOM	0.669	0.818	<0.001	0.686	0.828	<0.001	0.682	0.826	<0.001
D9_SOT	0.743	0.862	<0.001	0.790	0.889	<0.001	0.769	0.877	<0.001
D10_TSW	0.740	0.860	<0.001	0.787	0.887	<0.001	0.766	0.875	<0.001
D11_YOR	0.642	0.801	<0.001	0.672	0.820	<0.001	0.658	0.811	<0.001
D12_ZUL	0.746	0.864	<0.001	0.794	0.891	<0.001	0.773	0.879	<0.001
D13_PIM	0.785	−0.886	<0.001	0.814	−0.902	<0.001	0.799	−0.894	<0.001
D14_ALE	0.814	−0.902	<0.001	0.837	−0.915	<0.001	0.824	−0.908	<0.001
D15_KAZ	0.028	−0.167	0.362	0.057	−0.238	0.156	0.036	−0.189	0.283
D16_MON	0.645	−0.803	<0.001	0.694	−0.833	<0.001	0.664	−0.815	<0.001
D17_LOK	0.071	−0.266	0.141	0.117	−0.342	0.038	0.085	−0.291	0.095
D18_CHU	0.762	−0.873	<0.001	0.797	−0.893	<0.001	0.774	−0.880	<0.001
D19_THA	0.199	−0.446	0.011	0.250	−0.500	0.002	0.217	−0.466	0.005
D20_VIE	0.255	−0.505	0.003	0.300	−0.548	<0.001	0.271	−0.521	0.002
D21_JAP	0.462	−0.680	<0.001	0.493	−0.702	<0.001	0.473	−0.688	<0.001
D22_MAL	0.141	−0.376	0.034	0.190	−0.436	0.007	0.159	−0.399	0.020
D23_PHI	0.181	−0.426	0.015	0.231	−0.481	0.003	0.200	−0.447	0.008
D24_BOR	0.183	−0.428	0.015	0.234	−0.484	0.002	0.202	−0.449	0.008
D25_AUN	0.114	−0.337	0.059	0.158	−0.398	0.015	0.130	−0.361	0.036
D26_NBR	0.107	−0.327	0.068	0.152	−0.390	0.017	0.123	−0.351	0.042
D27_NEP	0.002	−0.042	0.819	0.011	−0.107	0.529	0.004	−0.062	0.727
D28_GRK	0.003	−0.051	0.781	0.021	−0.144	0.394	0.007	−0.086	0.630
D29_ITY	0.002	−0.046	0.804	0.020	−0.141	0.404	0.007	−0.082	0.646
D30_KBR	0.004	−0.062	0.737	0.024	−0.155	0.360	0.009	−0.096	0.588
D31_FIN	0.021	−0.144	0.432	0.057	−0.239	0.154	0.032	−0.180	0.309
D32_LAP	0.042	−0.205	0.261	0.086	−0.294	0.078	0.057	−0.238	0.175
Da_EHol							0.712	0.844	<0.001
Da_SHol							0.771	0.878	<0.001
Da_EHM				0.724	0.851	<0.001			
Da_EHE				0.689	0.830	<0.001			
Da_SHL				0.789	0.888	<0.001			
Da_SHM				0.790	0.889	<0.001			
Da_SHE				0.790	0.889	<0.001			

MDS = multidimensional scaling; MMD = mean measure of divergence.
[a] See text for details.

limitations of the latter, prompted us to discuss findings from the matched pooled African samples first. Even then, given their still-small sample sizes and uneven geographic and temporal distribution, results from these ancient genetic data are interpreted cautiously and are used primarily to assess concordance with phenetic patterns, rather than as standalone evidence of population relationships. Our conclusions based on individual ancient and recent dental data are presented afterward.

Phenetically, Da_EHol shows very low levels of differentiation (Table 5) from East African Kenya D3_KKU and Somalia D8_SOM. Somali ancestors lived within that region since the Late Pleistocene/Early Holocene (Brandt, 1988; Reid et al., 2019), but the Kenyan Kikuyu link seemed surprising. Relative to the date range of Da_EHol, 10,000–2950 BP, ancestors of Bantu-speaking Kikuyu did not reach Kenya before ~2000 BP (Clist, 1987; Ashley, 2010). That said, their contact with indigenous East Africans may have contributed to this affinity, as implied by 'Bantu' ancestry in some Somalis (see Fig. 1a in Chen et al., 2024), and the F_{ST} results (mentioned afterward). Moreover, the MDS plot (Fig. 4A) conveys important nuance. Da_EHol is closer to D8_SOM than D3_KKU and nearest to North Africans along dimension 2—consistent with the documented Eurasian pastoralist ancestry (Lazaridis et al., 2016; Skoglund et al., 2017; Wang et al., 2020). D3_KKU is actually plotted closer to the other 'Bantu' samples (D9_SOT, D10_TSW, and D12_ZUL) from South Africa. In this region, Da_SHol is likewise akin to the recent Khoesan, D4_RRI and D5_SAN. Da_EHol and Da_SHol differ significantly from each other. All told, these pooled results imply continuity within East and South Africa from the Holocene through recent periods, with a phenetic divide between regions that decreased through time (SOM Table S3), for the reasons presented afterward.

With their larger sizes than the individual ancient samples, Ga_EHol and Ga_SHol—especially the former—delivered F_{ST} distances (Table 6) more comparable in magnitude to those between recent African and other global samples (SOM Table S4). Ga_EHol again has the closest affinity to East African G3_KKU and G8_SOM (Table 9), though it is at some distance from them on dimension 2 of the MDS plot (Fig. 4B). Instead, it is again positioned closer to the North Africans, likely reflecting the Eurasian ancestry. Of all F_{ST} distances, the lowest ones for Ga_SHol are with South African Khoesan G4_KHO and G5_JUH. This too is evident in the MDS plot, with Ga_SHol located some distance away, but at least within their general vicinity.

Thus, while still strong due to the affinities among recent matched samples, the Mantel correlation between these MMD and F_{ST} matrices is lower (Table 7) than mentioned earlier. And, while the correlation between MMD and minimum-slope matrices actually increased, that between F_{ST} and corresponding geographic distances is lower. In any event, both Figure 4 MDS plots again take on a clinal configuration, identifying marked dental and genetic diversity within Africa—including pooled South African Da_SHol and Ga_SHol on the left of dimension 1 in their respective plots—before the transition to Eurasian and other global samples.

As such, coefficients of determination remain high comparing pooled and recent samples. Regressing MDS dimension 1 coordinates from Da_EHol and Da_SHol (Fig. 4A) on minimum-slope distances slightly increased the R^2 value of all recent dental samples. Values 0.71 and 0.77 are comparable for Da_EHol and Da_SHol (Table 8; Fig. 8A, B), respectively. For matching comparative genetic samples Ga_EHol and Ga_SHol (Table 9), the trend is in the same regional direction, but the disparity in R^2 values is greater (0.62 and 0.78, respectively). The outlier status of Ga_SHol is obvious in regression plots (Fig. 8C, D). Adding ancient genetic samples more variedly and negatively affected the R^2 values of recent samples. For both genetic samples, corresponding R^2 values in Africa and the farthest dispersal extent (Northern Siberia/Americas) decreased substantially. Yet, despite limitations of these two pooled genetic samples, overall correspondence with dental output reinforces the validity of the latter to further address our first research question. Indeed, ASUDAS data provide greater accuracy and reliability than low-coverage aDNA from these still-small samples.

Following on from our pooled analyses, the five individual ancient East and South African dental samples are again phenetically similar to later peoples within each region (Table 5). This is irrespective of the fact that, beyond a few cases in Da_SHL, all dentitions comprising them are 2000–12,000 years older than recent Sub-Saharan samples. So, the claim that ASUDAS traits are evolutionarily conservative to facilitate diachronic study is supported, along with an increase in the correlation between MMD and minimum slope when adding the five ancient samples (0.76).

The small, insignificant MMD distances of Da_EHM and Da_EHE with Kenya (D3_KKU) and Somalia (D8_SOM) offer temporal evidence that this phenetic link extends from at least the Early Holocene through recent times. As noted, these two ancient East African samples also show affinities to other recent Sub-Saharan samples, except South African Khoesan and Zulu. Also, in the north, both, especially the more recent Da_EHM, share a relatively

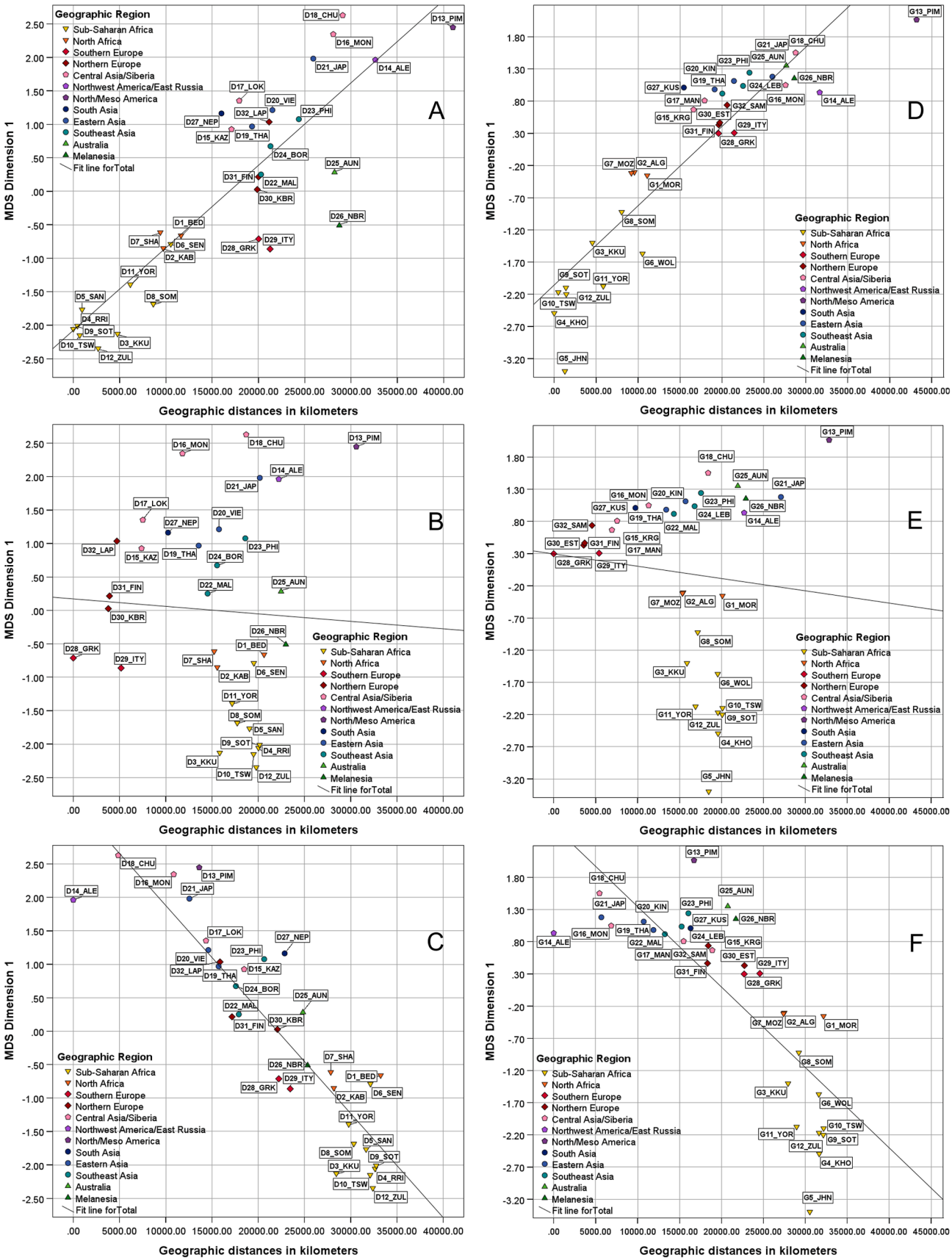

Figure 6. Multidimensional scaling dimension 1 coordinates regressed against geographic distances for 32 recent global dental (A–C) and genetic (D–F) samples. Exemplar plots show range of coefficients of determination between Africa—the geographic origin, an intermediate location, and the farthest extent of dispersal in this study. Dental samples: A) D4_RRI, South Africa ($R^2 = 0.74$, $p < 0.01$), B) D28_GRK, Greece ($R^2 < 0.01$, $p = 0.78$), and C) D14_ALE, Aleutian Islands ($R^2 = 0.81$, $p < 0.01$). Genetic samples: D) G4_KHO, South

Table 9
Regression results for MDS dimension 1 of F_{ST} matrix against geographic distances for the recent and recent/pooled ancient genetic sample analyses,[a] listing coefficients of determination (R^2), correlations (r), and *p* values.

Analysis	Recent			Recent and Pooled		
Sample	R^2	r	*p*	R^2	r	*p*
G1_MOR	0.569	0.754	<0.001	0.484	0.696	<0.001
G2_ALG	0.490	0.700	<0.001	0.411	0.641	<0.001
G3_KKU	0.704	0.839	<0.001	0.621	0.788	<0.001
G4_KHO	0.830	0.911	<0.001	0.773	0.879	<0.001
G5_JHN	0.821	0.906	<0.001	0.748	0.865	<0.001
G6_WOL	0.585	0.765	<0.001	0.498	0.706	<0.001
G7_MOZ	0.504	0.710	<0.001	0.423	0.650	<0.001
G8_SOM	0.645	0.803	<0.001	0.554	0.744	<0.001
G9_SOT	0.832	0.912	<0.001	0.762	0.873	<0.001
G10_TSW	0.832	0.912	<0.001	0.767	0.876	<0.001
G11_YOR	0.694	0.833	<0.001	0.607	0.779	<0.001
G12_ZUL	0.826	0.909	<0.001	0.755	0.869	<0.001
G13_PIM	0.585	−0.765	<0.001	0.546	−0.739	<0.001
G14_ALE	0.637	−0.798	<0.001	0.612	−0.782	<0.001
G15_KRG	0.011	−0.106	0.565	0.025	−0.159	0.369
G16_MON	0.599	−0.774	<0.001	0.599	−0.774	<0.001
G17_MAN	0.054	−0.233	0.199	0.080	−0.283	0.105
G18_CHU	0.530	−0.728	<0.001	0.523	−0.723	<0.001
G19_THA	0.289	−0.538	0.001	0.315	−0.561	<0.001
G20_KIN	0.377	−0.614	<0.001	0.393	−0.627	<0.001
G21_JAP	0.392	−0.626	<0.001	0.386	−0.621	<0.001
G22_MAL	0.287	−0.536	0.002	0.310	−0.557	<0.001
G23_PHI	0.297	−0.545	0.001	0.316	−0.562	<0.001
G24_LEB	0.308	−0.555	<0.001	0.326	−0.571	<0.001
G25_AUN	0.296	−0.544	0.001	0.307	−0.554	<0.001
G26_NBR	0.292	−0.540	0.001	0.303	−0.550	<0.001
G27_KUS	0.030	−0.172	0.345	0.050	−0.224	0.203
G28_GRK	0.010	−0.098	0.595	0.023	−0.152	0.391
G29_ITY	0.011	−0.104	0.571	0.025	−0.157	0.375
G30_EST	0.011	−0.106	0.562	0.025	−0.159	0.368
G31_FIN	0.039	−0.198	0.279	0.062	−0.248	0.157
G32_SAM	0.046	−0.215	0.237	0.070	−0.265	0.131
Ga_EHol				0.615	0.784	<0.001
Ga_SHol				0.783	0.885	<0.001

F_{ST} = Hudson FST distance matrix; MDS = multidimensional scaling.
[a] See text for details.

low MMD with the geographically closest non-African sample, i.e., southern European D28_GRK (Table 5). This not only is consistent with an East African origin for global dispersal but also reflects shared ancestry from Eurasian pastoralist back-migration (Lazaridis et al., 2016; Skoglund et al., 2017; Wang et al., 2020). Lastly, significant differences exist between the two East and three South African ancient samples (Table 5) to reinforce inter-regional distinctiveness during the Holocene (SOM Table S3). However, increased temporal resolution revealed a steady decrease in MMD distances between samples from these regions, notably Da_EHE (Table 5), from the Early to Middle to Late Holocene.

In South Africa, Da_SHL, Da_SHM, and Da_SHE are akin to recent Khoesan (Table 5). But MMD distances from these individual samples now show a resemblance to Sotho (D9_SOT) and Tswana (D10_TSW). This is not surprising as Khoesan and Bantu-speaking peoples experienced considerable admixture (Henn et al., 2011; May et al., 2013; Montinaro et al., 2017; Sengupta et al., 2021) since the latter reached South Africa in the 1st–2nd centuries AD (Klapwijk and Huffman, 1996; Antonites, 2016). Sub-Saharan Africans have the highest frequencies of key traits that add crown mass and root complexity relative to other populations—specifically Bushman upper canine, Carabelli's M^1, two-rooted P^1, three-rooted M^2, M^3 presence, M_2 Y-groove, M_1 cusp 7, P_1 Tome's root, and two-rooted M_2—while possessing the lowest frequencies of I^1 double shovel and M^1 enamel extension (Irish, 1997). Collectively, this suite of 11 traits is termed 'Afridonty' (Irish, 2013) and, in this combination of prevalence, was recognized as plesiomorphic (ancestral) among populations (Irish, 1997, 1998a; Irish and Guatelli-Steinberg, 2003). Both of the recent South African groups (SOM Table S1; Irish, 2016), especially the Khoesan, prominently express this pattern and share low, insignificant intersample MMD distances (SOM Table S3).

The MDS configuration (Fig. 3) visualized all of these relationships but, again, effectively shows broader among-sample trends in accord with known population history. On dimension 2, three sample groupings are evident top to bottom: 1) recent North Africans, 2) Holocene and recent East, West, and South (i.e., 'Bantu') Africans, and 3) Holocene and recent Khoesan from South Africa. North Africans, who trend toward a simpler mass-reduced crown morphology (Irish, 1998b), plot next to dentally simpler Europeans and fairly near Afridont Da_EHM and Da_EHE—in accord with the Eurasian-related gene flow into North and East Africa during the Holocene (Ramachandran et al., 2005; Lazaridis et al., 2016; Skoglund et al., 2017; Wang et al., 2020; Bergström et al., 2021; Fan et al., 2023). Correspondingly, of all Sub-Saharan Africans, European samples—especially D28_GRK from Greece—are nearest to Da_EHM and Da_EHE on dimension 2. The latter two are, in turn, closer to Somalis (D8_SOM) than the Kenyans (D3_KKU). The Kenyan sample is near the West African Yoruba (D11_YOR) and, again, South African D9_SOT, D10_TSW, and D12_ZUL, from the southward expansion of Bantu speakers (May et al., 2013; Montinaro et al., 2017; Sengupta et al., 2021). To the south, the most recent ancient sample, Late Holocene Da_SHL, is closest to the recent Khoesan, followed successively by older Da_SHM and Da_SHE to imply isolation by time (Konigsberg, 1990; Duforet-Frebourg and Slatkin, 2016). As mentioned earlier, such configurations may reflect ordination of clinal data; therefore, interpretation focuses on relative positioning along the gradient rather than the geometric form of the distribution itself.

Low MMD distances between the Holocene and recent regional African samples further elevated the R^2 value (Table 8; Fig. 7), with the latter higher in the two ancient East ($\geq$0.69) and particularly three South African samples ($\geq$0.79). These reflect strong IBD signals preserved in both regions and demographic remnants of restricted gene flow and cumulative reductions in population size during range expansion (DeGiorgio et al., 2009; Deshpande et al., 2009). Building on established spatial genetic gradients (Wright, 1943; Cavalli-Sforza et al., 1994; Relethford, 2004), our findings continue to align with genomic research showing decreasing diversity and increasing divergence with greater distance from Africa (Prugnolle et al., 2005; Ramachandran et al., 2005; Li et al., 2008; Jay et al., 2013; Kanitz et al., 2018; Tobler et al., 2023). At the level of individual traits—and paralleling neutral genomic structure—the distribution of ASUDAS variants likewise follows this pattern (Irish, 1997, 1998a; Irish and Guatelli-Steinberg, 2003; Hanihara, 2008; Scott et al., 2018).

Nevertheless, causes of the global dental trait distribution appear to be more complex. South and North European samples and, to a lesser extent, South Asia D27_NEP from Nepal, exhibit an overall reduction in variation, random frequency shifts, and loss of complex Afridont traits (SOM Tables S1 and S2), as expected from the dispersal bottleneck and later founder events. All also have higher MMD distances with geographic distance (SOM Table S3 and S5). Europeans exhibit reduced crown complexity and fewer accessory cusps and roots, termed Eurodonty, while South Asians

Africa (R^2 = 0.74, p < 0.01), E) G28_GRK, Greece (R^2 < 0.01, p = 0.60), and F) G14_ALE, Aleutian Islands (R^2 = 0.64, p < 0.01). Details are mentioned in the text and in Tables 1, 2, 8, and 9. (For interpretation of the references to color in this figure, the reader is referred to the web version of this article.)

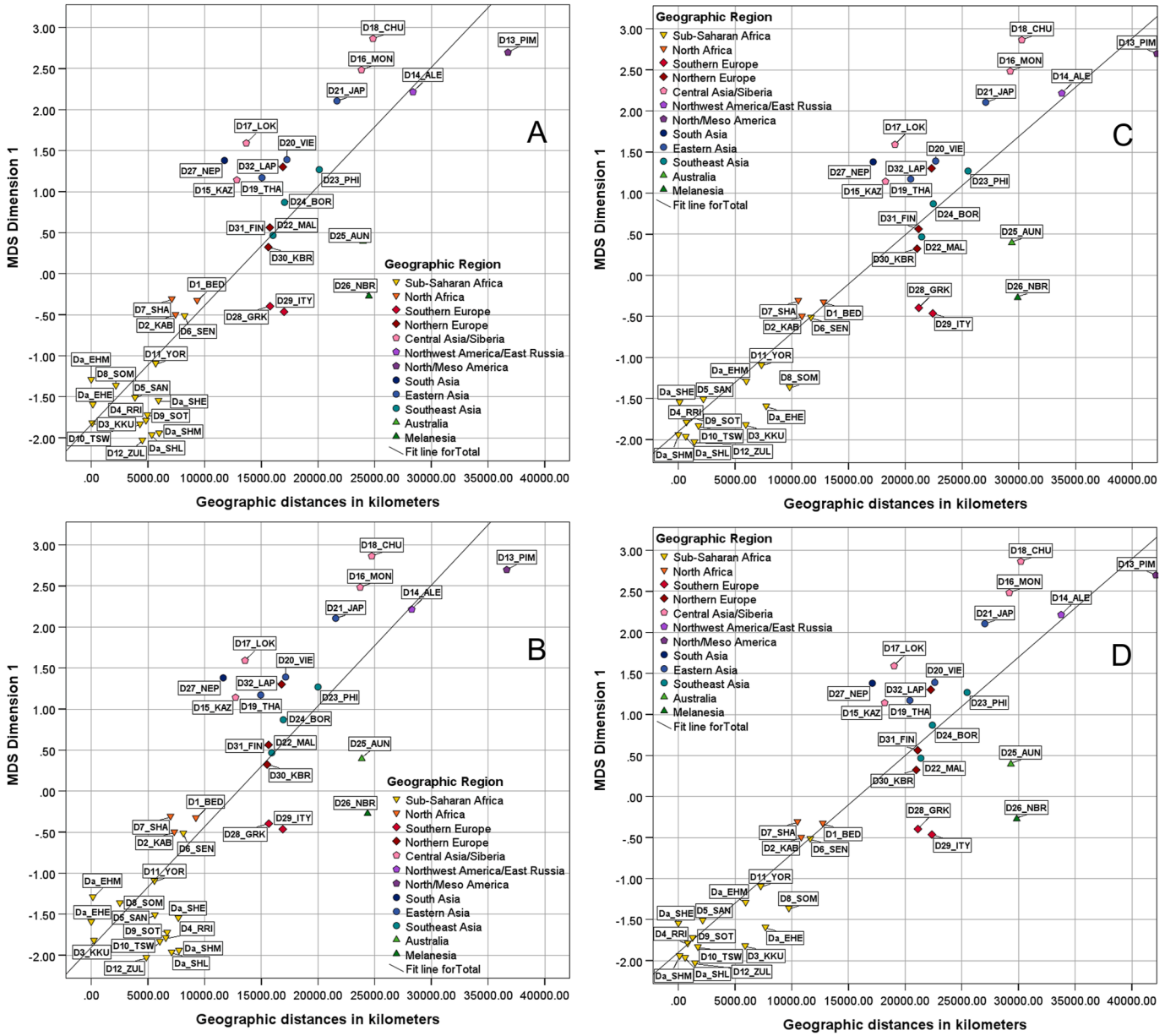

Figure 7. Multidimensional scaling dimension 1 coordinates regressed against geographic distances for 32 recent global and five ancient Sub-Saharan African dental samples. Plots show coefficients of determination for Middle and Early Holocene East and South African samples relative to others. A) Da_EHM, East Africa ($R^2 = 0.72$), B) Da_EHE, East Africa ($R^2 = 0.69$), C) Da_SHM, South Africa ($R^2 = 0.79$), and D) Da_SHE, South Africa ($R^2 = 0.79$). Details are mentioned in text and in Tables 1 and 8 (For interpretation of the references to color in this figure, the reader is referred to the web version of this article.)

show intermediate patterns with regional variability designated as Indodonty (for a list of key high-frequency traits, see Hawkey, 2004; Scott et al., 2018). These among-population differences reflect long-term divergence, drift, and population history, while contributing to the phenetic distances among global samples in our analyses. However, the proximity of Melanesian sample D26_NBR to Sub-Saharan Africans in MDS plots and low MMDs relative to geographic separation do not follow this gradation. The position of D26_NBR below the lines of fit lends support (e.g., Fig. 7). Its relatively elevated frequencies of various ancestral Afridont traits (SOM Table S2) explain this association (Irish, 1997, 1998a, 2013).

Seeming morphogenetic similarities have long been reported between African and Sahul populations (Giblett, 1969; Howells, 1989; Turner, 1992; Cavalli-Sforza et al., 1994; Scott et al., 2018). Explanations have ranged from parallel selection (Nurse et al., 1985) to symplesiomorphy (Stringer et al., 1997). That said, "the linkage… is neither intuitively satisfying nor supported by any archaeological evidence" (Turner, 1992:149), and recent genomic findings are likewise not supportive (e.g., Malaspinas et al., 2016; also see Fig. 2B).

Another hypothesis is that these similarities reflect early dispersal history. The founding population(s) reached Sahul rapidly, with Australia occupied ~50,000–65,000 BP (Clarkson et al., 2017) and genetic evidence for matching dates in Melanesia (Pedro et al., 2020). By chance, the founders may have retained ancestral dental trait frequencies like those in Africa, with ensuing long-term geographic and reproductive isolation maintaining them. In the remaining non-African populations, founder effects, drift, and admixture reduced these traits.

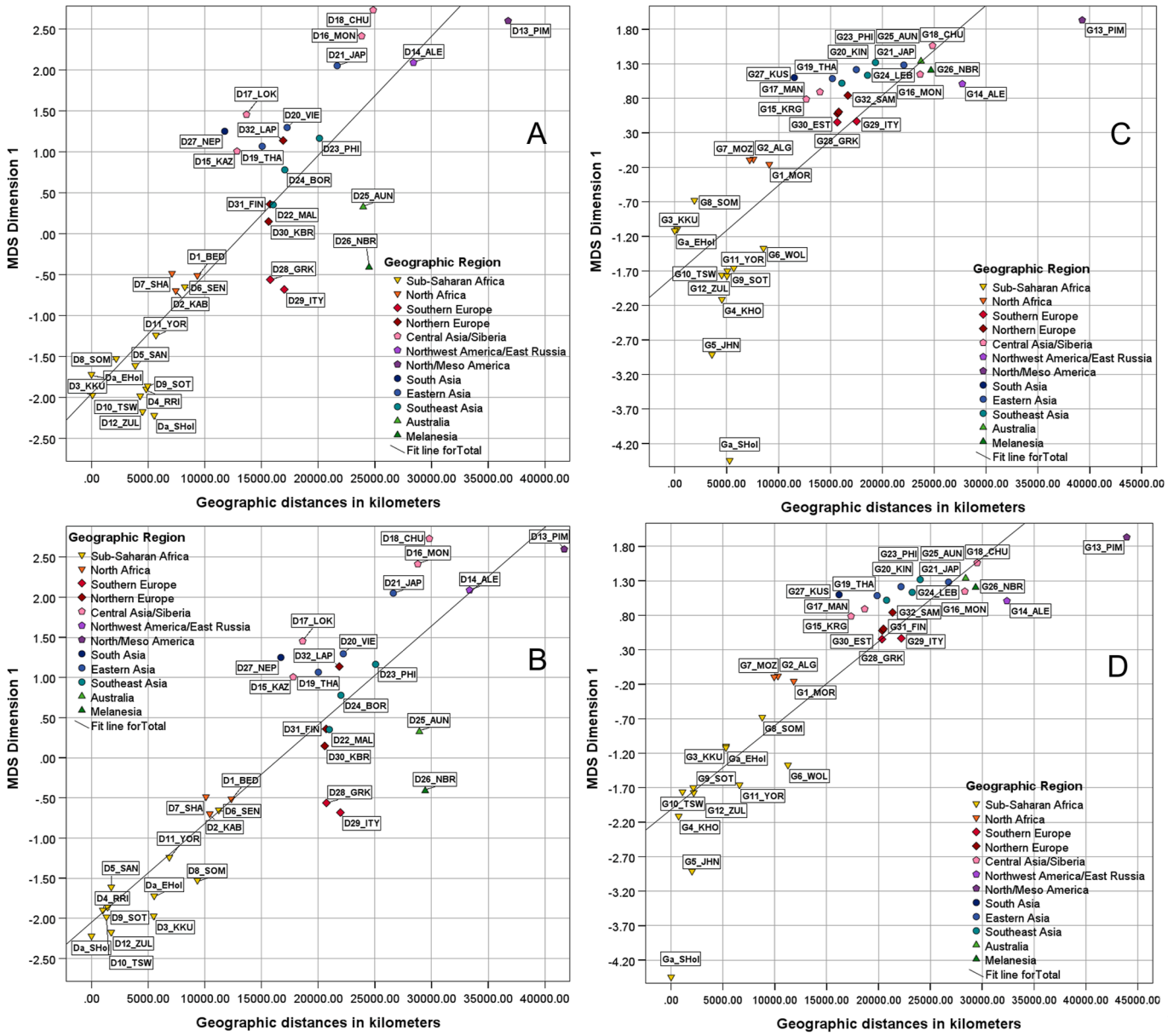

Figure 8. Multidimensional scaling dimension 1 coordinates regressed against geographic distances for 32 recent global and two ancient Sub-Saharan African pooled dental (A, B) and genetic (C, D) samples. Plots show coefficients of determination for Holocene East and South Africa relative to the rest. Dental samples: A) Da_EHol, East Africa ($R^2 = 0.71$) and B) Da_SHol, South Africa ($R^2 = 0.77$). Genetic samples: C) Ga_EHol, East Africa ($R^2 = 0.62$) and D) Ga_SHol, South Africa ($R^2 = 0.78$). See text and Tables 1, 2, 8, and 9. (For interpretation of the references to color in this figure, the reader is referred to the web version of this article.)

An additional possibility is that Denisovan introgression contributed to the Sahul dental patterns, including potential similarities with Sub-Saharan Africans in retaining ancestral mass-additive traits. However, based on the limited dental evidence available, large molars and distinct root traits of Denisovans do not closely match the Afridont pattern, suggesting limited influence (Zubova et al., 2017; Chen et al., 2019; Demeter et al., 2022; Tsutaya et al., 2025).

Finally, selection may have played an incidental role. Genes in broader developmental systems (e.g., WNT10A, MSX1, and PAX9) can influence general dental morphology (van den Boogaard et al., 2000; Galluccio et al., 2012; Kimura et al., 2015; Dhamo et al., 2016). But one gene in particular, EDAR, has a documented secondary effect on certain ASUDAS traits. Melanesians and nearby populations retain the ancestral V370V genotype at frequencies like those of Africans and Europeans (Bryk et al., 2008; Malaspinas et al., 2016; Santos et al., 2016). The derived V370A allele, which promotes expression of alternate traits, is essentially absent.

The V370A variant is thought to have originated ~30,000–35,000 years ago in East Asia; it rose in frequency after the LGM and reached very high levels by the early Holocene (Sabeti et al., 2007; Bryk et al., 2008; Kamberov et al., 2013; Hlusko et al., 2018; Mao et al., 2021; Zhang et al., 2022). Evidence indicates that selection primarily targeted alterations in hair and in sweat, sebaceous, and mammary glands (Kimura et al., 2009; Park et al., 2012; Kamberov et al., 2013; Kataoka et al., 2021). However, EDAR regulates a broader developmental pathway, so changes indirectly influenced dental morphology through pleiotropy. This resulted in high frequencies of I^1 shoveling and double shoveling, possibly contributed to I^1 winging (in response to increased anterior tooth size), and was linked to additional lower molar

cusps. Conversely, the frequencies of double-rooted P^1 and M_2 decreased significantly, but that of three-rooted M_1 increased (Kimura et al., 2009; Park et al., 2012; Kamberov et al., 2013; Kataoka et al., 2021). These are all hallmark traits of Sinodonty (Turner, 1990b), a pattern most common in Northeast Asia and the Americas. In contrast, Southeast Asians have lower frequencies of EDAR V370A and correspondingly fewer derived crown and root traits—a pattern that Turner (1990b) termed Sundadonty—which further illustrates how different dispersal histories yielded distinct yet related dental complexes.

That said, while some traits are influenced through pleiotropy (Kimura et al., 2009; Park et al., 2012; Hlusko et al., 2018), global dental variation still appears to be largely shaped by drift, founder effects, and demographic structure (Scott et al., 2018); this includes Sinodonty, which comprises several other high-frequency traits (Turner, 1990b) not tied to V370A. Another factor involves shared developmental pathways that can generate intertrait covariance (Hillson, 1996; Jernvall and Jung, 2000; Jernvall and Thesleff, 2012). However, these pathways are conserved across global populations, so trait distributions generally align with neutral genomic structure. Therefore, despite some biological complexities, ASUDAS traits behave in a broadly neutral-like manner at large geographic scales, with an acknowledgment that developmental integration and pleiotropic genetic effects may influence expression and covariance of individual traits.

4.2. Within Africa

Our discussion concludes by focusing on the 12 modern (Table 1) and five ancient African dental samples (Table 3) to explore areas of influence and origin within the continent since the Late Pleistocene. Again, MMD distances (SOM Table S3; Table 5) revealed several key trends. First, long-term differences are suggested between the North and Sub-Saharan Africans. Second, a decrease in variation is observed through time between Early through Late Holocene peoples of South and East Africa. Third, extended continuity is evident in the latter regions, along with documented population movements. These results pertain to our second research question: East and South African Holocene samples are phenetically akin to their recent regional counterparts. So, sustained population stability coupled with intermittent contact across Sub-Saharan Africa in the Holocene is implied to build a foundation for later population structure evidenced by genetic and morphological data.

Figure 3 provides visualization of these affinities, but for finer detail, an African-only MDS configuration was generated (Fig. 9). The south-north distribution, now on dimension 1, remains associated with geographic locale but with increased variation among and within the three main sample groupings. Additional nuance is present along dimension 2, namely, separation between West and East Africans, as well as Holocene/Khoesan and 'Bantu' in South Africa. In support, a Mantel test between MMD and least slope distance matrices for all 12 samples yielded $r_m = 0.69$ ($p < 0.01$). While not reaching the strength of correlation for all 37 samples (Table 7), which was likely influenced by sample number and intercontinental distances, it too is strongly positive.

Regression analyses of all 37 dental samples also show this intra-African patterning (Table 8). The highest R^2 values are in South Africans, then lower in the West and East, and lowest in the North. To enhance detail, we regressed MDS dimension 1 coordinates from Figure 9 against the minimum-slope distances within Africa. The R^2 values (Table 10) and residuals distributed

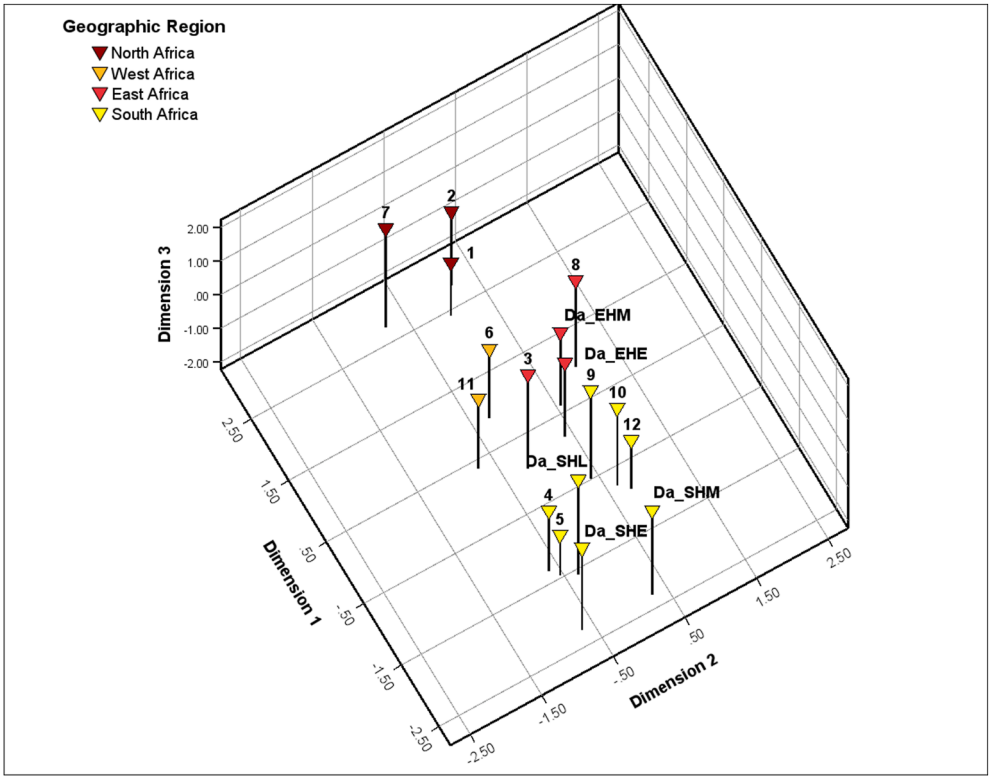

Figure 9. Multidimensional scaling plot of MMD distances among the 12 recent and five ancient Sub-Saharan African dental samples. Multidimensional scaling statistics indicate borderline good fit of the solution (stress = 0.10, $R^2 = 0.95$) Numbers refer to sample abbreviations in Table 1. Da_EHM = East African Middle Holocene, Da_EHE = East African Early Holocene, Da_SHL = South African Late Holocene, Da_SHM = South African Middle Holocene, Da_SHE = South African Early Holocene. Details are mentioned in Table 3 and text. MMD = mean measure of divergence. (For interpretation of the references to color in this figure, the reader is referred to the web version of this article.)

Table 10
Regression results for MDS dimension 1 of MMD matrix against geographic distances for recent/ancient African dental sample analyses,[a] listing coefficients of determination (R^2), correlations (r), and *p* values.

Sample	R^2	r	*p*
D1_BED	0.712	−0.844	<0.001
D2_KAB	0.835	−0.914	<0.001
D3_KKU	0.066	0.256	0.322
D4_RRI	0.821	0.906	<0.001
D5_SAN	0.757	0.870	<0.001
D6_SEN	0.584	−0.764	<0.001
D7_SHA	0.757	−0.870	<0.001
D8_SOM	0.003	−0.053	0.839
D9_SOT	0.796	0.892	<0.001
D10_TSW	0.778	0.882	<0.001
D11_YOR	0.130	−0.360	0.156
D12_ZUL	0.764	0.874	<0.001
Da_EHM	0.057	0.239	0.355
Da_EHE	0.000	−0.021	0.938
Da_SHL	0.848	0.921	<0.001
Da_SHM	0.854	0.924	<0.001
Da_SHE	0.856	0.925	<0.001

MDS = multidimensional scaling; MMD = mean measure of divergence.
[a] See text for details.

along the line of fit again reflect 'orientation of the main dispersal axis,' with information about the origin and farthest extent of dispersal (Ponce de León et al., 2018:5). Of course, this 'origin' does not represent the source of global dispersal but those Sub-Saharan samples with the greatest dental diversity. Holocene and recent Khoesan have the highest occurrence of ancestral, mass-additive crown and root traits that epitomize Afridonty (Irish, 1997, 1998a, 2013; Irish and Guatelli-Steinberg, 2003). Regression plots (Fig. 10) show Da_SHE, the most ancient South African sample, with the highest R^2 value (0.86, $p < 0.01$), followed in chronological order by Da_SHM, Da_SHL, the recent Khoesan, and 'Bantu.' West and East Africans are lowest, e.g., Da_EHE (0.01, $p = 0.94$), with North Africans again high (e.g., D2_KAB; 0.84, $p < 0.01$), returning an inverse IBD signal.

This south-north axis likely reflects a combination of Pleistocene and Holocene population movements. The distinctive dental trait frequencies observed mesh with genetic findings that position southern Sub-Saharan ancient and recent Khoesan populations as among the earliest diverging branches of all modern human genetic diversity (Henn et al., 2011; Schlebusch et al., 2017; Skoglund et al., 2017; Jakobsson et al., 2025). This is compatible with evidence that Late Pleistocene Africans formed a regionally structured but interconnected metapopulation in which southern, western, and eastern lineages diverged several hundred thousand years ago yet continued some gene exchange over time (Skoglund and Mathieson, 2018; Chan et al., 2019; Rito et al., 2019; Wang et al., 2020; Hollfelder et al., 2021; Wilkins, 2021; Fan et al., 2023; Ragsdale et al., 2023; Hallett et al., 2025; Jakobsson et al., 2025). Divergence among these regions, shaped by climate shifts and periodic admixture (Bergström et al., 2021; Hollfelder et al., 2021; Fan et al., 2023), produced a long-standing spatial population structure that lasted into the Holocene.

Ensuing Holocene demographic processes would have further contributed to the south-north gradient. East African groups of heterogeneous ancestry expanded southward during the Middle-Late Holocene (Skoglund et al., 2017; Rito et al., 2019; Wang et al., 2020). After that, the so-called 'Bantu expansion' provided additional gene flow from north to south (May et al., 2013; Montinaro et al., 2017; Sengupta et al., 2021). These events reshaped variation across regions but would not entirely erase earlier population signatures. Thus, the gradient in dental variation captures effects of both enduring Pleistocene population structure and Holocene exchanges.

Against this backdrop, southern Africa appears repeatedly as a key biogeographic center. Archaeological and paleoenvironmental studies found evidence of continual habitation, including occupation of the Makgadikgadi-Okavango paleo-wetland in Botswana for >70,000 years, and of major behavioral and technological innovations in the Kalahari Basin and along coastal refugia (Henshilwood et al., 2011; Brown et al., 2012; Clark and Kandel, 2013; Backwell et al., 2018; Chan et al., 2019; Wilkins, 2021; Will et al., 2023). Mitochondrial data suggest basal L0–L1 lineages diversified in the south before spreading north during the interglacial periods (Rito et al., 2019), linking southern peoples to those involved in later expansions, including Out-of-Africa II dispersal (Prugnolle et al., 2005; Ramachandran et al., 2005; Manica et al., 2007; Bergström et al., 2021; Hallett et al., 2025). Jay et al. (2013) likewise detected a south-north axis of genetic variation consistent with successive expansions.

This patterning, as evidenced by 1) population contraction and overlap of divergent forager lineages (Wang et al., 2020) and 2) protracted connectivity across ecosystems (Hollfelder et al., 2021; Fan et al., 2023) indicates that African population structure was ancient but had altered through time relative to climate, mobility, and cultural change (Skoglund et al., 2017; Rito et al., 2019; Fan et al., 2023; Hallett et al., 2025). All told, this combined history bears directly on our third research question, i.e., whether the south-north gradient in dental variation mirrors documented intra-African genetic clines that developed before, and were later modified after, the Late Pleistocene dispersal from East Africa.

Together, these cross-disciplinary findings link phenetic gradients in ASUDAS traits with genetic, archaeological, and paleoenvironmental evidence. Clines in dental trait frequencies within Africa reveal regional variation from processes outlined earlier. They also identify the broader Late Pleistocene dispersal signal, i.e., increasing divergence with geographic distance, global contrasts in dental expression, and spatial configurations expected under IBD and serial founder effects. Because these traits are evolutionarily conservative and unaffected by the taphonomic and coverage limitations of aDNA, they provide a continuous morphological record that complements genomic reconstructions of the initial dispersal from Africa and subsequent global differentiation. Overall, structured population continuity within Africa, with contributions from the south, generated the phenotypic and genetic bases from which non-Sub-Saharan populations derived (Bergström et al., 2021; Fan et al., 2023; Ragsdale et al., 2023). An East African origin is recognized, but the dental trait results—along with genetic and other evidence—underscore the broader subcontinental population structure from which that dispersal ultimately emerged. The patterns align with genetic and archaeological evidence for structured but interconnected African populations while not excluding alternative demographic scenarios that could produce similar spatial gradients.

5. Summary and conclusions

We employed 25 ASUDAS traits within a model-free framework to examine global population structure, emphasizing the Late Pleistocene Out-of-Africa II dispersal and population dynamics in the continent. Building on our earlier work (Irish et al., 2020), we added five Early through Late Holocene dental samples from East and South Africa, matched with comparative ancient genetic datasets, and applied a novel minimum-slope geographic distance measure to estimate more realistic dispersal paths. Using MMD distances from a total 37 dental samples ($n = 3167$) compared with Hudson's F_{ST} in genetic samples ($n = 566$), we assessed how dental

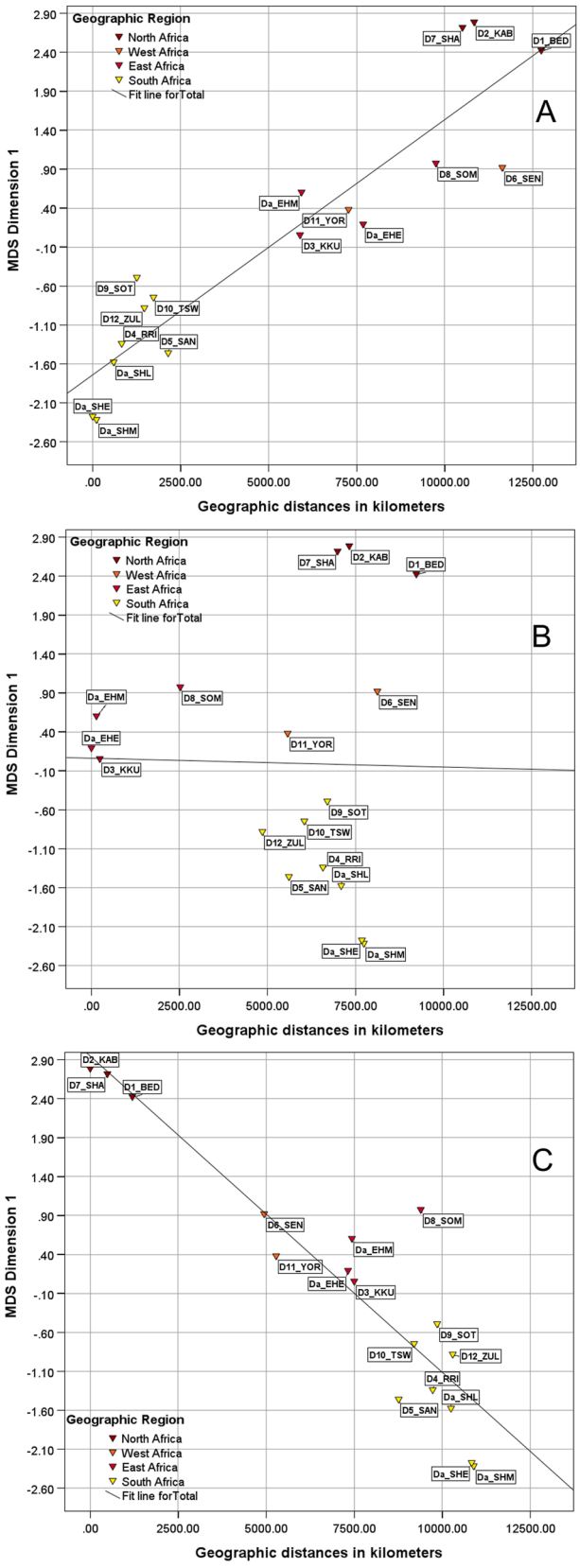

Figure 10. Multidimensional scaling dimension 1 coordinates regressed against geographic distances for the 12 recent and five ancient Sub-Saharan African dental samples defined in Tables 1 and 3. Plots show coefficients of determination for three exemplar samples: A) Da_SHE, South Africa (R^2 = 0.86), B) Da_EHE, East Africa (R^2 < 0.01), and C) D2_KAB, North Africa (R^2 = 0.84). See text and Table 10. (For interpretation of the references to color in this figure, the reader is referred to the web version of this article.)

variation parallels patterns seen in neutral genomic structure with Mantel tests, MDS, and regressions of MDS coordinates on minimum-slope distances.

First, we assessed whether MMD corresponds with F_{ST} distances. The strong correlations among them and their minimum-slope distances suggest ASUDAS traits emulate neutral genetic structure (Irish et al., 2020). Both dental and genetic MDS plots visualize a clinal configuration consistent with IBD and declining diversity at greater geographic distances from Africa (Prugnolle et al., 2005; Ramachandran et al., 2005; Betti et al., 2009). Our findings support the interpretation that ASUDAS traits preserve deep-time indications of population structure and can act as reliable proxies when aDNA has low coverage or is not preserved.

Second, we established whether Early-Late Holocene dental samples from East and South Africa evidenced phenetic continuity with recent regional populations. Pooled and individual ancient East African samples differed insignificantly from recent Kenyans and Somalis. As well, the ancient South African samples closely resembled recent Khoesan, implying isolation by time. The results support long-term population continuity within regions, with intermittent gene flow across Sub-Saharan Africa (Skoglund et al., 2017; Hollfelder et al., 2021; Fan et al., 2023). The ancient East and South African samples differ significantly from one another, but a reduction in magnitude of pairwise MMD distances over time suggests increased inter-regional connectivity during the later Holocene. So, these dental sample affinities further reinforce that ASUDAS traits are evolutionarily conservative and support diachronic analyses.

Third, we asked if a south-north gradient in dental variation parallels known genetic clines within Africa. Regressing dental MDS dimension 1 coordinates against minimum-slope distances yielded the highest R^2 value in South African Holocene and recent samples, notably the oldest (Da_SHE, 0.86). This echoes genetic evidence of a south-north axis and deep population structure (Jay et al., 2013; Kanitz et al., 2018; Ragsdale et al., 2023; Jakobsson et al., 2025). Of all populations, South African Khoesan retains the highest frequencies of ancestral traits characterizing Afridonty (Irish, 1997, 1998a, 2013) and the greatest genetic diversity (Henn et al., 2011; Skoglund et al., 2017; Jakobsson et al., 2025), aligning with archaeological and paleoenvironmental evidence for a prolonged occupation, ecological stability, and technological innovation in the area (Henshilwood et al., 2011; Brown et al., 2012; Backwell et al., 2018; Wilkins, 2021; Will et al., 2023). These patterns were modified by later Holocene demographics, namely the southward movement of East African pastoralists and 'Bantu expansion,' introducing additional population structure and contact across regions without erasing deeper phenetic signatures (e.g., Montinaro et al., 2017; Rito et al., 2019; Wang et al., 2020; Sengupta et al., 2021). Therefore, while East Africa is the acknowledged source of Out-of-Africa II (Ramachandran et al., 2005; Kanitz et al., 2018; Lipson et al., 2022), the deep diversity retained in the south, together with long-standing connections across the continent helped shape the demographic and cultural foundations from which global dispersion ultimately proceeded.

Several limitations remain to be addressed. The ancient genetic data were constrained by very small samples and missing data, which contributed to inflated F_{ST} values and unstable MDS configurations. Pooling the ancient samples by region improved the correspondence between dental, genetic, and geographic matrices but still fell short of the resolution achieved with dental data.

These genetic data were used primarily for comparative purposes. Still, more ancient dental samples, especially from West and Central Africa, and higher-coverage ancient genomes will help refine estimates of intra-African structure and improve future paired dental-genomic analyses. Ultimately, matched dental and genetic data from the same individuals remain the ideal for fully integrating morphological and genomic perspectives.

In sum, our results show that ASUDAS traits can act as reliable neutral-like markers that preserve deep spatial and temporal signs of population structure. Combined dental, genetic, and geographic evidence supports a model of enduring, structured population continuity across Africa, with South Africa maintaining marked diversity and East Africa providing the demographic source for global dispersal. This highlights dental morphology as an independent line of evidence complementing genomic, archaeological, and paleoenvironmental data.

Declaration of competing interest

J.D.I. has nothing to declare; A.M.J. has nothing to declare; J.M.L. has nothing to declare; L.G.F. has nothing to declare; G.R.S. has nothing to declare.

Acknowledgments

We thank all individuals at institutions, past and present, from which dental data were collected. Gareth Weedall of Liverpool John Moores University provided valuable assistance to A.M.J. during the bioinformatics processing of genomic data, especially realignment and processing of the Wolof raw data. Finally, we acknowledge the efforts of Christy G. Turner II, who worked for decades developing methods for using dental morphology in population studies and amassed the world's largest database on tooth crown and root variation on a global scale. J.D.I.: National Science Foundation (BCS-0840674, BNS-0104731, BNS-9013942), Arizona State University Research Development Program, and American Museum of Natural History.

Author contributions

Joel D. Irish: Writing – review & editing, Writing – original draft, Resources, Project administration, Methodology, Investigation, Funding acquisition, Formal analysis, Data curation, Conceptualization. **Adeline Morez Jacobs:** Writing – review & editing, Writing – original draft, Methodology, Formal analysis, Conceptualization. **James M. Lea:** Writing – review & editing, Writing – original draft, Methodology, Formal analysis, Conceptualization. **Linus Girdland Flink:** Writing – review & editing, Methodology. **G. Richard Scott:** Writing – review & editing, Methodology, Data curation.

Declaration of generative AI and AI-assisted technologies in the manuscript preparation process

During the preparation of this work the author(s) used ChatGPT 5.2 in order to find potential relevant (and real) research articles for inclusion. After using this tool/service, the author(s) reviewed and edited the content as needed and take(s) full responsibility for the content of the published article.

Data availability statement

Frequencies used for calculating mean measure of divergence distances are provided in the manuscript and supplemental online materials. SNP data are publically available as cited.

Supplementary Online Material

Supplementary Online Material related to this article can be found at https://doi.org/10.1016/j.jhevol.2026.103855.

References

Abbas, M., Lai, Z., Jansen, J.D., Tu, H., Alqudah, M., Xu, X., Al-Saqarat, B.S., Al Hseinat, M.A., Ou, X., Petraglia, M.D., Carling, P.A., 2023. Human dispersals out of Africa via the Levant. Sci. Adv. 9 (40), eadi6838.
Antonites, A., 2016. The organization of salt production in early first millennium CE South Africa. J. Anthropol. Archaeol. 44, 31–42.
Ashley, C.Z., 2010. Towards a socialised archaeology of ceramics in Great Lakes Africa. Afr. Archaeol. Rev. 27 (2), 135–163.
Atkinson, Q.D., 2011. Phonemic diversity supports a serial founder effect model of language expansion from Africa. Science 332, 346–349.
Backwell, L., Bradfield, J., Carlson, K.J., Jashashvili, T., Wadley, L., d'Errico, F., 2018. The antiquity of bow-and-arrow technology: Evidence from Middle Stone Age layers at Sibudu Cave. Antiquity 92 (362), 289–303.
Bailey, G., Cawthra, H.C., 2023. The significance of sea-level change and ancient submerged landscapes in human dispersal and development: A geo-archaeological perspective. Oceanologia 65 (1), 50–70.
Bergström, A., Stringer, C., Hajdinjak, M., Scerri, E.M.L., Skoglund, P., 2021. Origins of modern human ancestry. Nature 590 (7845), 229–237.
Betti, L., Balloux, F., Amos, W., Hanihara, T., Manica, A., 2009. Distance from Africa, not climate, explains within-population phenotypic diversity in humans. Proc. Biol. Sci. 276 (1658), 809–814.
Beyer, R.M., Krapp, M., Eriksson, A., Manica, A., 2021. Climatic windows for human migration out of Africa in the past 300,000 years. Nat. Commun. 12 (1), 4889.
Bhatia, G., Patterson, N., Sankararaman, S., Price, A.L., 2013. Estimating and interpreting F_{ST}: The impact of rare variants. Genome Res. 23, 1514–1521.
Brandt, S.A., 1988. Early Holocene mortuary practices and hunter-gatherer adaptations in southern Somalia. World Archaeol. 20 (1), 40–56.
Briggs, A.W., Stenzel, U., Meyer, M., Krause, J., Kircher, M., Pääbo, S., 2010. Removal of deaminated cytosines and detection of in vivo methylation in ancient DNA. Nucleic Acids Res. 38 (6), e87.
Bryk, J., Hardouin, E., Pugach, I., Hughes, D., Strotmann, R., Stoneking, M., Myles, S., 2008. Positive selection in East Asians for an EDAR allele that enhances NF-κB activation. PLoS One 3 (5), e2209.
Brown, K.S., Marean, C.W., Jacobs, Z., Schoville, B.J., Oestmo, S., Fisher, E.C., Bernatchez, J., Karkanas, P., Matthews, T., 2012. An early and enduring advanced technology originating 71,000 years ago in South Africa. Nature 491 (7425), 590–593.
Cavalli-Sforza, L.L., Menozzi, P., Piazza, A., 1994. The History and Geography of Human Genes. Princeton University Press, Princeton.
Chan, E.K., Timmermann, A., Baldi, B.F., Moore, A.E., Lyons, R.J., Lee, S.S., Kalsbeek, A.M., Petersen, D.C., Rautenbach, H., Förtsch, H.E., Bornman, M.R., 2019. Human origins in a southern African palaeo-wetland and first migrations. Nature 575 (7781), 185–189.
Chen, F., Welker, F., Shen, C.-C., Bailey, S.E., Bergmann, I., Davis, S., Xia, H., Wang, H., Fischer, R., Freidline, S.E., Yu, T.-L., Skinner, M.M., Stelzer, S., Dong, G., Fu, Q., Dong, G., Wang, J., Zhang, D., Hublin, J.-J., 2019. A late Middle Pleistocene Denisovan mandible from the Tibetan Plateau. Nature 569 (7756), 409–412.
Chen, S., Lei, C., Zhao, X., Pan, Y., Lu, D., Xu, S., 2024. AncestryPainter 2.0: Visualizing ancestry composition and admixture history graph. Genome Biol. Evol. 16 (11), evae249.
Clark, J.L., Kandel, A.W., 2013. The evolutionary implications of variation in human hunting strategies and diet breadth during the Middle Stone Age of southern Africa. Curr. Anthropol. 54 (S8), S269–S287.
Clarkson, C., Jacobs, Z., Marwick, B., Fullagar, R., Wallis, L., Smith, M., Roberts, R.G., Hayes, E., Lowe, K., Carah, X., Florin, S.A., 2017. Human occupation of northern Australia by 65,000 years ago. Nature 547 (7663), 306–310.
Clist, B., 1987. Early Bantu settlements in west-central Africa: A review of recent research. Curr. Anthropol. 28 (3), 380–382.
Dhamo, B., Fennis, W., Créton, M., Vucic, S., Cune, M., Ploos van Amstel, H.K., Wolvius, E.B., van den Boogaard, M.J., Ongkosuwito, E.M., 2016. The association between WNT10A variants and dental development in patients with isolated oligodontia. Eur. J. Hum. Genet. 25 (1), 59–65.
DeGiorgio, M., Jakobsson, M., Rosenberg, N.A., 2009. Explaining worldwide patterns of human genetic variation using a coalescent-based serial founder model of migration outward from Africa. Proc. Natl. Acad. Sci. U.S.A. 106 (38), 16057–16062.
Demeter, F., Zanolli, C., Westaway, K.E., Joannes-Boyau, R., Duringer, P., Morley, M.W., Welker, F., Rüther, P.L., Skinner, M.M., McColl, H., Gaunitz, C., Vinner, L., Dunn, T.E., Olsen, J.V., Sikora, M., Ponche, J.-L., Suzzoni, E., Frangeul, S., Boesch, Q., Antoine, P.-O., Pan, L., Xing, S., Zhao, J.-X., Bailey, R.M., Boualaphane, S., Sichanthongtip, P., Sihanam, D., Patole-Edoumba, E., Aubaile, F., Crozier, F., Bourgon, N., Zachwieja, A., Luangkhoth, T., Souksavatdy, V., Sayavongkhamdy, T., Cappellini, E., Bacon, A.-M., Hublin, J.-J., Willerslev, E., Shackelford, L., 2022. A Middle Pleistocene Denisovan molar from the Annamite Chain of northern Laos. Nat. Commun. 13 (1), 2557.

Deshpande, O., Batzoglou, S., Feldman, M.W., Cavalli-Sforza, L.L., 2009. A serial founder effect model for human settlement out of Africa. Proc. Biol. Sci. 276 (1655), 291–300.
Duforet-Frebourg, N., Slatkin, M., 2016. Isolation-by-distance-and-time in a stepping-stone model. Theor. Popul. Biol. 108, 24–35.
Dugard, P., Todman, J., Staines, H., 2022. Multidimensional scaling. In: Approaching Multivariate Analysis, 2nd ed. Routledge, London, pp. 263–285.
Fan, S., Spence, J.P., Feng, Y., Hansen, M.E., Terhorst, J., Beltrame, M.H., Ranciaro, A., Hirbo, J., Beggs, W., Thomas, N., Nyambo, T., 2023. Whole-genome sequencing reveals a complex African population demographic history and signatures of local adaptation. Cell 186 (5), 923–939.
Frichot, E., Schoville, S., Bouchard, G., François, O., 2012. Correcting principal component maps for effects of spatial autocorrelation in population genetic data. Front. Genet. 3, 254.
Galluccio, G., Castellano, M., La Monaca, C., 2012. Genetic basis of non-syndromic anomalies of human tooth number. Arch. Oral Biol. 57 (7), 918–930.
Garcea, E.A., 2010. Bridging the gap between in and out of Africa. In: Garcea, E.A. (Ed.), South-eastern Mediterranean Peoples Between 130,000 and 10,000 Years Ago. Oxbow Books, pp. 174–182.
GEBCO Compilation Group, 2024. GEBCO Grid. https://doi.org/10.5285/1c44ce99-0a0d-5f4f-e063-7086abc0ea0f.
Giblett, E.R., 1969. Genetic Markers in Human Blood. Blackwell, Oxford.
Gorelick, N., Hancher, M., Dixon, M., Ilyushchenko, S., Thau, D., Moore, R., 2017. Google earth engine: Planetary-scale geospatial analysis for everyone. Rem. Sens. Environ. 202, 18–27.
Gowan, E.J., Zhang, X., Khosravi, S., Rovere, A., Stocchi, P., Hughes, A.L., Gyllencreutz, R., Mangerud, J., Svendsen, J.I., Lohmann, G., 2021. A new global ice sheet reconstruction for the past 80,000 years. Nat. Commun. 12 (1), 1199.
Green, R.F., Suchey, J.M., 1976. The use of inverse sine transformations in the analysis of non-metric cranial data. Am. J. Phys. Anthropol. 45, 61–68.
Gretzinger, J., Gibbon, V.E., Penske, S.E., Sealy, J.C., Rohrlach, A.B., Salazar-García, D.C., Krause, J., Schiffels, S., 2024. 9,000 years of genetic continuity in southernmost Africa demonstrated at Oakhurst rockshelter. Nat. Ecol. Evol. 8 (11), 2121–2134.
Guillot, G., Rousset, F., 2013. Dismantling the Mantel tests. Methods Ecol. Evol. 4, 336–344.
Hallett, E.Y., Leonardi, M., Cerasoni, J.N., Will, M., Beyer, R., Krapp, M., Kandel, A.W., Manica, A., Scerri, E.M., 2025. Major expansion in the human niche preceded out of Africa dispersal. Nature 644, 115–121.
Hammer, Ø., Harper, D.A., Ryan, P.D., 2001. PAST: Paleontological statistics software package for education and data analysis. Palaeontol. Electron. 4 (1), 9.
Hanihara, T., 2008. Morphological variation of major human populations based on nonmetric dental traits. Am. J. Phys. Anthropol. 136, 169–182.
Hanihara, T., 2013. Geographic structure of dental variation in the major human populations of the world. Anthropolog. Perspect. Tooth Morphol. 66, 479.
Hawkey, D.E., 2004. The Peopling of South Asia: Evidence for Affinities and Microevolution of Prehistoric Populations of India and Sri Lanka. National Museums of Colombo, Colombo, Sri Lanka.
Henn, B.M., Gignoux, C.R., Feldman, M.W., Mountain, J.L., 2011. Genetic evidence for recent population mixture in Africa. Proc. Natl. Acad. Sci. 108 (13), 5154–5159.
Henshilwood, C.S., d'Errico, F., Van Niekerk, K.L., Coquinot, Y., Jacobs, Z., Lauritzen, S.E., Menu, M., García-Moreno, R., 2011. A 100,000-year-old ochre-processing workshop at Blombos Cave, South Africa. Science 334 (6053), 219–222.
Higgins, D., Hughes, T.E., James, H., Townsend, G.C., 2009. Strong genetic influence on hypocone expression of permanent maxillary molars in South Australian twins. Dental Anthropol. J. 22, 1–7.
Hillson, S., 1996. Dental Anthropology. Cambridge University Press, Cambridge.
Hlusko, L.J., Carlson, J.P., Chaplin, G., Elias, S.A., Hoffecker, J.F., Huffman, M., Jablonski, N.G., Monson, T.A., O'Rourke, D.H., Pilloud, M.A., Scott, G.R., 2018. Environmental selection during the last ice age on the mother-to-infant transmission of vitamin D and fatty acids through breast milk. Proc. Natl. Acad. Sci. 115 (19), E4426–E4432.
Hollfelder, N., Breton, G., Sjödin, P., Jakobsson, M., 2021. The deep population history in Africa. Hum. Mol. Genet. 30 (R1), R2–R10.
Howells, W.W., 1989. Skull Shapes and the Map: Craniometric analyses in the Aispersion of Modern *Homo*. In: Papers of the Peabody Museum of Archaeology and Ethnology, vol. 79. Harvard University, Cambridge, MA.
Hublin, J.J., 2021. How old are the oldest *Homo sapiens* in Far East Asia? Proc. Natl. Acad. Sci. 118 (10), e2101173118.
Hublin, J.J., Sirakov, N., Aldeias, V., Bailey, S., Bard, E., Delvigne, V., Endarova, E., Fagault, Y., Fewlass, H., Hajdinjak, M., Kromer, B., 2020. Initial Upper Palaeolithic *Homo sapiens* from Bacho Kiro Cave, Bulgaria. Nature 581 (7808), 299–302.
Hudson, R.R., Slatkin, M., Maddison, W.P., 1992. Estimation of levels of gene flow from DNA sequence data. Genetics 132, 583–589.
Hughes, T.E., Townsend, G.C., 2011. Twin studies of dental crown morphology: Genetic and environmental determinants of the Cusp of Carabelli'. In: Program of the 15th International Symposium on Dental Morphology, Newcastle, UK, 25 August, p. 37.
Hughes, T.E., Townsend, G.C., 2013. Twin and family studies of human dental crown morphology: Genetic, epigenetic, and environmental determinants of the modern human dentition. In: Scott, G.R., Irish, J.D. (Eds.), Anthropological Perspectives on Tooth Morphology: Genetics, Evolution, Variation. Cambridge University Press, Cambridge, pp. 31–68.
Hughes, T., Townsend, G., Bockmann, M., 2016. An overview of dental genetics. In: Irish, J.D., Scott, G.R. (Eds.), A Companion to Dental Anthropology. Wiley-Blackwell, New York, pp. 123–141.
Irish, J.D., 1993. Biological affinities of Late Pleistocene through Modern African aboriginal populations: The dental evidence. Ph.D. Dissertation, Arizona State University, Tempe.
Irish, J.D., 1997. Characteristic high- and low-frequency dental traits in sub-Saharan African populations. Am. J. Phys. Anthropol. 102 (4), 455–467.
Irish, J.D., 1998a. Ancestral dental traits in recent sub-Saharan Africans and the origins of modern humans. J. Hum. Evol. 34 (1), 81–98.
Irish, J.D., 1998b. Diachronic and synchronic dental trait affinities of Late and post-Pleistocene peoples from North Africa. Homo 49, 138–155.
Irish, J.D., 2000. The Iberomaurusian enigma: North African progenitor or dead end? J. Hum. Evol. 39, 393–410.
Irish, J.D., 2005. Population continuity versus discontinuity revisited: dental affinities among Late Paleolithic through Christian era Nubians. Am. J. Phys. Anthropol. 128, 520–535.
Irish, J.D., 2006. Who were the ancient Egyptians? Dental affinities among Neolithic through post- dynastic peoples. Am. J. Phys. Anthropol. 129, 529–543.
Irish, J.D., 2010. The mean measure of divergence (MMD): Its utility in model-free and model-bound analyses relative to the Mahalanobis D2 distance for nonmetric traits. Am. J. Hum. Biol. 22, 378–395.
Irish, J.D., 2013. Afridonty: The "sub-Saharan African Dental Complex" revisited. In: Scott, G.R., Irish, J.D. (Eds.), Anthropological Perspectives on Tooth Morphology: Genetics, Evolution, Variation. Cambridge University Press, Cambridge, pp. 278–295.
Irish, J.D., 2016. Who were they really? Model-free and model-bound dental nonmetric analyses to affirm documented population affiliations of seven South African "Bantu" samples. Am. J. Phys. Anthropol. 159, 655–670.
Irish, J.D., Black, W., Sealy, J., Ackermann, R.R., 2014. Questions of Khoesan continuity: Dental affinities among the indigenous Holocene peoples of South Africa. Am. J. Phys. Anthropol. 155, 33–44.
Irish, J.D., Guatelli-Steinberg, D., 2003. Ancient teeth and modern human origins: An expanded comparison of African Plio-Pleistocene and recent world dental samples. J. Hum. Evol. 45 (2), 113–144.
Irish, J.D., Lillios, K.T., Waterman, A.J., Silva, A.M., 2017. Other" possibilities? Assessing regional and extra-regional dental affinities of populations in the Portuguese Estremadura to explore the roots of Iberia's Late Neolithic-Copper Age. J. Archaeolog. Sci.: Rep. 11, 224–236.
Irish, J.D., Morez, A., Girdland Flink, L., Phillips, E.L., Scott, G.R., 2020. Do dental nonmetric traits actually work as proxies for neutral genomic data? Some answers from continental- and global-level analyses. Am. J. Phys. Anthropol. 172 (3), 347–375.
Irish, J.D., Usai, D., 2021. The transition from hunting–gathering to agriculture in Nubia: Dental evidence for and against selection, population continuity and discontinuity. Proc. R. Soc. B 288 (1952), 20210969.
Jakobsson, M., Bernhardsson, C., McKenna, J., Hollfelder, N., Vicente, M., Edlund, H., Coutinho, A., Sjödin, P., Brink, J., Zipfel, B., Malmström, H., 2025. *Homo sapiens*-specific evolution unveiled by ancient southern African genomes. Nature 3, 1–8.
Jay, F., Sjödin, P., Jakobsson, M., Blum, M.G., 2013. Anisotropic isolation by distance: The main orientations of human genetic differentiation. Mol. Biol. Evol. 30 (3), 513–525.
Jernvall, J., Thesleff, I., 2012. Tooth shape formation and tooth renewal: Evolving with the same signals. Development 139, 3487–3497.
Jernvall, J., Jung, H.S., 2000. Genotype, phenotype, and developmental biology of molar tooth characters. Yearbk. Phys. Anthropol. 43, 171–190.
Kamberov, Y.G., Wang, S., Tan, J., Gerbault, P., Wark, A., Tan, L., Yang, Y., Li, S., Tang, K., Chen, H., Powell, A., 2013. Modeling recent human evolution in mice by expression of a selected EDAR variant. Cell 152 (4), 691–702.
Kanitz, R., Guillot, E.G., Antoniazza, S., Neuenschwander, S., Goudet, J., 2018. Complex genetic patterns in humans arise from a simple range-expansion model over continental landmasses. PLoS One 13 (2), e0192460.
Kataoka, K., Fujita, H., Isa, M., Gotoh, S., Arasaki, A., Ishida, H., Kimura, R., 2021. The human EDAR 370V/A polymorphism affects tooth root morphology potentially through the modification of a reaction–diffusion system. Sci. Rep. 11 (1), 5143.
Kimura, R., Yamaguchi, T., Takeda, M., Kondo, O., Toma, T., Haneji, K., Hanihara, T., Matsukusa, H., Kawamura, S., Maki, K., Osawa, M., 2009. A common variation in EDAR is a genetic determinant of shovel-shaped incisors. Am. J. Hum. Genet. 85, 528–535.
Kimura, R., Watanabe, C., Kawaguchi, A., Takeda, M., Haneji, K., Yamaguchi, T., 2015. Common polymorphisms in WNT10A affect tooth morphology as well as hair shape. Hum. Mol. Genet. 24 (9), 2673–2680.
Klapwijk, M., Huffman, T.N., 1996. Excavations at Silver Leaves: A final report. S. Afr. Archaeol. Bull. 51 (164), 84–93.
Konigsberg, L.W., 1990. Analysis of prehistoric biological variation under a model of isolation by geographic and temporal distance. Hum. Biol. 62, 49–70.
Kruskal, J.B., Wish, M., 1978. Multidimensional scaling (No. 11). Sage Publications, Newbury Park.
Langgut, D., Almogi-Labin, A., Bar-Matthews, M., Pickarski, N., Weinstein-Evron, M., 2018. Evidence for a humid interval at~ 56–44 ka in the Levant and

its potential link to modern human dispersal out of Africa. J. Hum. Evol. 124, 75–90.
Lawson Handley, L.J., Perrin, N., 2007. Advances in our understanding of mammalian sex-biased dispersal. Mol. Ecol. 16 (8), 1559–1578.
Lazaridis, I., Nadel, D., Rollefson, G., Merrett, D.C., Rohland, N., Mallick, S., Fernandes, D., Novak, M., Gamarra, B., Sirak, K., Connell, S., 2016. Genomic insights into the origin of farming in the ancient Near East. Nature 536 (7617), 419–424.
Lazaridis, I., Patterson, N., Mittnik, A., Renaud, G., Mallick, S., Kirsanow, K., Sudmant, P.H., Schraiber, J.G., Castellano, S., Lipson, M., Berger, B., 2014. Ancient human genomes suggest three ancestral populations for present-day Europeans. Nature 513 (7518), 409–413.
Leakey, L.S.B., 1970. The Stone Age Races of Kenya, Second Edition. Oxford University Press, London.
Legendre, P., Fortin, M.-J., 2010. Comparison of the Mantel test and alternative approaches for detecting complex multivariate relationships in the spatial analysis of genetic data. Mol. Ecol. Resour. 10, 831–844.
Li, J.Z., Absher, D.M., Tang, H., Southwick, A.M., Casto, A.M., Ramachandran, S., Cann, H.M., Barsh, G.S., Feldman, M., Cavalli-Sforza, L.L., Myers, R.M., 2008. Worldwide human relationships inferred from genome-wide patterns of variation. Science 319 (5866), 1100–1104.
Lipson, M., Sawchuk, E.A., Thompson, J.C., Oppenheimer, J., Tryon, C.A., Ranhorn, K.L., De Luna, K.M., Sirak, K.A., Olalde, I., Ambrose, S.H., Arthur, J.W., 2022. Ancient DNA and deep population structure in sub-Saharan African foragers. Nature 603 (7900), 290–296.
Malaspinas, A.-S., Westaway, M.C., Muller, C., Sousa, V.C., Lao, O., Alves, I., Bergström, A., Athanasiadis, G., Cheng, J.Y., Crawford, J.E., Heupink, T.H., Macholdt, E., Peischl, S., Rasmussen, S., Schiffels, S., Subramanian, S., Wright, J.L., Albrechtsen, A., Barbieri, C., Dupanloup, I., Eriksson, A., Margaryan, A., Moltke, I., Pugach, I., Korneliussen, T.S., Levkivskyi, I., Moreno-Mayar, J.V., Ni, S., Racimo, F., Sikora, M., Stoneking, M., Schierup, M.H., Excoffier, L., Durbin, R., Nielsen, R., Manica, A., Lambert, D.M., Willerslev, E., Lahr, M.M., Kayser, M., 2016. A genomic history of Aboriginal Australia. Nature 538, 207–214.
Mallick, S., Li, H., Lipson, M., Mathieson, I., Gymrek, M., Racimo, F., Zhao, M., Chennagiri, N., Nordenfelt, S., Tandon, A., Skoglund, P., 2016. The Simons genome diversity project: 300 genomes from 142 diverse populations. Nature 538, 201.
Mallick, S., Micco, A., Mah, M., Ringbauer, H., Lazaridis, I., Olalde, I., Patterson, N., Reich, D., 2024. The Allen Ancient DNA Resource (AADR): A curated compendium of ancient human genomes. Sci. Data 11 (1), 1–10.
Manica, A., Prugnolle, F., Balloux, F., 2005. Geography is a better determinant of human genetic differentiation than ethnicity. Hum. Genet. 118 (3), 366–371.
Manica, A., Amos, W., Balloux, F., Hanihara, T., 2007. The effect of ancient population bottlenecks on human phenotypic variation. Nature 448 (7151), 346–348.
Mao, X., Zhang, H., Qiao, S., Liu, Y., Chang, F., Xie, P., Zhang, M., Wang, T., Li, M., Cao, P., Yang, R., 2021. The deep population history of northern East Asia from the Late Pleistocene to the Holocene. Cell 184 (12), 3256–3266.
Mathieson, I., Lazaridis, I., Rohland, N., Mallick, S., Patterson, N., Roodenberg, S.A., Harney, E., Stewardson, K., Fernandes, D., Novak, M., Sirak, K., 2015. Genome-wide patterns of selection in 230 ancient Eurasians. Nature 528 (7583), 499–503.
May, A., Hazelhurst, S., Li, Y., 2013. Genetic diversity in black South Africans from Soweto. BMC Genom. 14, 644.
Montinaro, F., Busby, G.B., Gonzalez-Santos, M., Oosthuitzen, O., Oosthuitzen, E., Anagnostou, P., Destro-Bisol, G., Pascali, V.L., Capelli, C., 2017. Complex ancient genetic structure and cultural transitions in southern African populations. Genetics 205 (1), 303–316.
Moreno-Mayar, J.V., Potter, B.A., Vinner, L., Steinrücken, M., Rasmussen, S., Terhorst, J., Kamm, J.A., Albrechtsen, A., Malaspinas, A.S., Sikora, M., Reuther, J.D., Irish, J.D., Malhi, R.S., Orlando, L., Song, Y.S., Nielsen, R., Meltzer, D.J., Willerslev, E., 2018. Terminal Pleistocene Alaskan genome reveals first founding population of Native Americans. Nature 553 (7687), 203–207.
Morton, J.T., Toran, L., Edlund, A., Metcalf, J.L., Lauber, C., Knight, R., 2017. Uncovering the horseshoe effect in microbial analyses. mSystems 2 (1), e00166-16.
Nicholson, S.L., Hosfield, R., Groucutt, H.S., Pike, A.W., Fleitmann, D., 2021. Beyond arrows on a map: The dynamics of *Homo sapiens* dispersal and occupation of Arabia during Marine Isotope Stage 5. J. Anthropol. Archaeol. 62, 101269.
Nikita, E., 2015. A critical review of the mean measure of divergence and Mahalanobis distances using artificial data and new approaches to the estimation of biodistances employing nonmetric traits. Am. J. Phys. Anthropol. 157 (2), 284–294.
Novembre, J., Stephens, M., 2008. Interpreting principal component analyses of spatial population genetic variation. Nat. Genet. 40 (5), 646–649.
Nurse, G.T., Weiner, J.S., Jenkins, T., 1985. The Peoples of Southern Africa and Their Affinities. Clarendon Press, Oxford.
Ortega-Del Vecchyo, D., Slatkin, M., 2019. F_{ST} between archaic and present-day samples. Heredity 122, 711–718.
Pagani, L., Lawson, D.J., Jagoda, E., Mörseburg, A., Eriksson, A., Mitt, M., Clemente, F., Hudjashov, G., DeGiorgio, M., Saag, L., Wall, J.D., 2016. Genomic analyses inform on migration events during the peopling of Eurasia. Nature 538 (7624), 238–242.
Park, J.H., Yamaguchi, T., Watanabe, C., Kawaguchi, A., Haneji, K., Takeda, M., Kim, Y.I., Tomoyasu, Y., Watanabe, M., Oota, H., Hanihara, T., 2012. Effects of an Asian-specific nonsynonymous EDAR variant on multiple dental traits. J. Hum. Genet. 57, 508.
Patterson, N., Moorjani, P., Luo, Y., Mallick, S., Rohland, N., Zhan, Y., Genschoreck, T., Webster, T., Reich, D., 2012. Ancient admixture in human history. Genetics 192 (3), 1065–1093.
Pedro, N., Brucato, N., Fernandes, V., Andre, M., Saag, L., Pomat, W., Besse, C., Boland, A., Deleuze, J.F., Clarkson, C., Sudoyo, H., Metspalu, M., Stoneking, M., Cox, M.P., Leavesley, M., Pereira, L., Ricaut, F.X., 2020. Papuan mitochondrial genomes and the settlement of Sahul. J. Hum. Genet. 65 (10), 875–887.
Pérez-Losada, J., Fort, J., 2023. Diffusion of humans out of Africa and the phonemic diversity cline. Diffusion Fundam. 38, 1–2.
Pickrell, J.K., Patterson, N., Barbieri, C., Berthold, F., Gerlach, L., Güldemann, T., Kure, B., Mpoloka, S.W., Nakagawa, H., Naumann, C., Lipson, M., 2012. The genetic prehistory of southern Africa. Nat. Commun. 3 (1), 1143.
Pickrell, J.K., Patterson, N., Loh, P.R., Lipson, M., Berger, B., Stoneking, M., Pakendorf, B., Reich, D., 2014. Ancient west Eurasian ancestry in southern and eastern Africa. Proc. Natl. Acad. Sci. 111 (7), 2632–2637.
Podani, J., Miklós, I., 2002. Resemblance coefficients and the horseshoe effect in principal coordinates analysis. Ecology 83, 3331–3343.
Ponce de León, M.S., Koesbardiati, T., Weissmann, J.D., Milella, M., Reyna-Blanco, C.S., Suwa, G., Kondo, O., Malaspinas, A.S., White, T.D., Zollikofer, C.P., 2018. Human bony labyrinth is an indicator of population history and dispersal from Africa. Proc. Natl. Acad. Sci. 115 (16), 4128–4133.
Prendergast, M.E., Lipson, M., Sawchuk, E.A., Olalde, I., Ogola, C.A., Rohland, N., Sirak, K.A., Adamski, N., Bernardos, R., Broomandkhoshbacht, N., Callan, K., 2019. Ancient DNA reveals a multistep spread of the first herders into sub-Saharan Africa. Science 365 (6448), eaaw6275.
Prugnolle, F., Manica, A., Balloux, F., 2005. Geography predicts neutral genetic diversity of human populations. Curr. Biol. 15 (5), R159–R160.
Ragsdale, A.P., Weaver, T.D., Atkinson, E.G., Hoal, E.G., Möller, M., Henn, B.M., Gravel, S., 2023. A weakly structured stem for human origins in Africa. Nature 617 (7962), 755–763.
Ramachandran, S., Deshpande, O., Roseman, C.C., Rosenberg, N.A., Feldman, M.W., Cavalli-Sforza, L.L., 2005. Support from the relationship of genetic and geographic distance in human populations for a serial founder effect originating in Africa. Proc. Natl. Acad. Sci. 102 (44), 15942–15947.
Reich, D., Patterson, N., Campbell, D., Tandon, A., Mazieres, S., Ray, N., Parra, M.V., Rojas, W., Duque, C., Mesa, N., García, L.F., 2012. Reconstructing Native American population history. Nature 488, 370–375.
Reid, R.E., Jones, M., Brandt, S., Bunn, H., Marshall, F., 2019. Oxygen isotope analyses of ungulate tooth enamel confirm low seasonality of rainfall contributed to the African Humid Period in Somalia. Palaeogeogr. Palaeoclimatol. Palaeoecol. 534, 109272.
Relethford, J., 2004. Global patterns of isolation by distance based on genetic and morphological data. Hum. Biol. 76 (4), 499–513.
Relethford, J.H., Harpending, H.C., 1994. Craniometric variation, genetic theory, and modern human origins. Am. J. Phys. Anthropol. 95, 249–270.
Reyes-Centeno, H., Rathmann, H., Hanihara, T., Harvati, K., 2017. Testing modern human out-of-Africa dispersal models using dental nonmetric data. Curr. Anthropol. 58 (S17), S406–S417.
Rito, T., Vieira, D., Silva, M., Conde-Sousa, E., Pereira, L., Mellars, P., Richards, M.B., Soares, P., 2019. A dispersal of *Homo sapiens* from southern to eastern Africa immediately preceded the out-of-Africa migration. Sci. Rep. 9 (1), 4728.
Sabeti, P.C., Varilly, P., Fry, B., Lohmueller, J., Hostetter, E., Cotsapas, C., Xie, X., Byrne, E.H., McCarroll, S.A., Gaudet, R., Schaffner, S.F., 2007. Genome-wide detection and characterization of positive selection in human populations. Nature 449 (7164), 913–918.
Saltré, F., Chadœuf, J., Higham, T., Ochocki, M., Block, S., Bunney, E., Llamas, B., Bradshaw, C.J., 2024. Environmental conditions associated with initial northern expansion of anatomically modern humans. Nat. Commun. 15 (1), 4364.
Santos, C., Phillips, C., Fondevila, M., Daniel, R., Van Oorschot, R.A., Burchard, E.G., Schanfield, M.S., Souto, L., Uacyisrael, J., Via, M., Carracedo, Á., 2016. Pacifiplex: An ancestry-informative SNP panel centred on Australia and the Pacific region. Forensic Sci. Int. Genet. 20, 71–80.
Schillaci, M.A., Irish, J.D., Wood, C.C., 2009. Further analysis of the population history of ancient Egyptians. Am. J. Phys. Anthropol. 139 (2), 235–243.
Schlebusch, C.M., Malmström, H., Günther, T., Sjödin, P., Coutinho, A., Edlund, H., Munters, A.R., Vicente, M., Steyn, M., Soodyall, H., Lombard, M., 2017. Southern African ancient genomes estimate modern human divergence to 350,000 to 260,000 years ago. Science 358 (6363), 652–655.
Scott, G.R., Irish, J.D., 2017. Human Tooth Crown and Root Morphology: The Arizona State University Dental Anthropology System. Cambridge University Press, Cambridge.
Scott, G.R., Turner, C.G.,I.I., Townsend, G.C., Martinón-Torres, M., 2018. The Anthropology of Modern Human Teeth: Dental Morphology and its Variation. Cambridge University Press, Cambridge.
Sengupta, D., Choudhury, A., Fortes-Lima, C., Aron, S., Whitelaw, G., Bostoen, K., Gunnink, H., Chousou-Polydouri, N., Delius, P., Tollman, S., Gómez-Olivé, F.X., 2021. Genetic substructure and complex demographic history of South African Bantu speakers. Nat. Commun. 12 (1), 2080.
Séré, M., Thévenon, S., Belem, A., De Meeûs, T., 2017. Comparison of different genetic distances to test isolation by distance between populations. Heredity 119, 55–63.
Shah, N., Meng, Q., Zou, Z., Zhang, X., 2024. Systematic analysis on the horse-shoe-like effect in PCA plots of scRNA-seq data. Bioinform. Adv. 4 (1), vbae109, 1–9.

Sokal, R.R., Rohlf, F.J., 1995. Biometry. Freeman and Company, New York.
Sjøvold, T., 1973. Occurrence of minor non-metrical variants in the skeleton and their quantitative treatment for population comparisons. Homo 24, 204–233.
Sjøvold, T., 1977. Non-metrical divergence between skeletal populations: The theoretical foundation and biological importance of C.A.B. Smith's mean measure of divergence. Ossa (Solna) 4 (Supplement 1), 1–133.
Skoglund, P., Mallick, S., Bortolini, M.C., Chennagiri, N., Hünemeier, T., Petzl-Erler, M.L., Salzano, F.M., Patterson, N., Reich, D., 2015. Genetic evidence for two founding populations of the Americas. Nature 525 (7567), 104–108.
Skoglund, P., Mathieson, I., 2018. Ancient genomics of modern humans: The first decade. Annu. Rev. Genom. Hum. Genet. 19, 381–404.
Skoglund, P., Posth, C., Sirak, K., Spriggs, M., Valentin, F., Bedford, S., Clark, G.R., Reepmeyer, C., Petchey, F., Fernandes, D., Fu, Q., 2016. Genomic insights into the peopling of the Southwest Pacific. Nature 538 (7626), 510–513.
Skoglund, P., Posth, C., Sirak, K., Spriggs, M., Valentin, F., Bedford, S., Clark, G.R., Reepmeyer, C., Petchey, F., Fernandes, D., Fu, Q., 2016. Genomic insights into the peopling of the Southwest Pacific. Nature 538, 510.
Skoglund, P., Thompson, J.C., Prendergast, M.E., Mittnik, A., Sirak, K., Hajdinjak, M., Salie, T., Rohland, N., Mallick, S., Peltzer, A., Heinze, A., 2017. Reconstructing prehistoric African population structure. Cell 171 (1), 59–71.
Smouse, P.E., Long, J.C., 1992. Matrix correlation analysis in anthropology and genetics. Am. J. Phys. Anthropol. 35 (S15), 187–213.
Soares, P., Alshamali, F., Pereira, J.B., Fernandes, V., Silva, N.M., Afonso, C., Costa, M.D., Musilová, E., Macaulay, V., Richards, M.B., Černý, V., 2012. The expansion of mtDNA haplogroup L3 within and out of Africa. Mol. Biol. Evol. 29 (3), 915–927.
Sołtysiak, A., 2011. An R script for Smith's mean measure of divergence. Bioarchaeol. Near East 5, 41–44.
Stringer, C.B., Humphrey, L.T., Compton, T., 1997. Cladistic analysis of dental traits in recent humans using a fossil outgroup. J. Hum. Evol. 32, 389–402.
Tobler, R., Souilmi, Y., Huber, C.D., Bean, N., Turney, C.S., Grey, S.T., Cooper, A., 2023. The role of genetic selection and climatic factors in the dispersal of anatomically modern humans out of Africa. Proc. Natl. Acad. Sci. 120 (22), e2213061120.
Tsutaya, T., Sawafuji, R., Taurozzi, A.J., Fagernäs, Z., Patramanis, I., Troché, G., Mackie, M., Gakuhari, T., Oota, H., Tsai, C.-H., Olsen, J.V., Kaifu, Y., Chang, C.-H., Cappellini, E., Welker, F., 2025. A male Denisovan mandible from Pleistocene Taiwan. Science 388 (6743), 176–180.
Turner II, C.G., 1985. The dental search for Native American origins. In: Kirk, R., Szathmary, E. (Eds.), Out of Asia. The Journal of Pacific History, Canberra, pp. 31–78.
Turner, C.G., 1990a. Origin and affinity of the people of Guam: A dental anthropological assessment. Micronesica Suppl. 2, 403–416.
Turner, C.G.I.I., 1990b. Major features of Sundadonty and Sinodonty, including suggestions about East Asian microevolution, population history, and late Pleistocene relationships with Australian aboriginals. Am. J. Phys. Anthropol. 82 (3), 295–317.
Turner, C.G.I.I., 1992. The dental bridge between Australia and Asia: Following Macintosh into the East Asian hearth of humanity. Archaeol. Ocean. 27, 143–152.
Turner, C.G.,I.I., Nichol, C.R., Scott, G.R., 1991. Scoring procedures for key morphological traits of the permanent dentition: The Arizona State University Dental Anthropology System. In: Kelley, M.A., Larsen, C.S. (Eds.), Advances in Dental Anthropology. Wiley-Liss, New York, pp. 13–31.
van den Boogaard, M.J.H., Dorland, M., Beemer, F.A., Ploos van Amstel, H.K., 2000. MSX1 mutation is associated with orofacial clefting and tooth agenesis in humans. Nat. Genet. 24 (4), 342–343.
Wang, K., Goldstein, S., Bleasdale, M., Clist, B., Bostoen, K., Bakwa-Lufu, P., Buck, L.T., Crowther, A., Dème, A., McIntosh, R.J., Mercader, J., 2020. Ancient genomes reveal complex patterns of population movement, interaction, and replacement in sub-Saharan Africa. Sci. Adv. 6 (24), eaaz0183.
Wilkins, J., 2021. *Homo sapiens* origins and evolution in the Kalahari Basin, southern Africa. Evol. Anthropol. 30 (5), 327–344.
Will, M., Kandel, A.W., Conard, N.J., 2023. Human behavioral variability and resilience in southern Africa during the Middle Stone Age. J. Hum. Evol. 178, 103341.
Wright, S., 1943. Isolation by distance. Genetics 28 (2), 114–138.
Yamazaki, D., Ikeshima, D., Tawatari, R., Yamaguchi, T., O'Loughlin, F., Neal, J.C., Sampson, C.C., Kanae, S., Bates, P.D., 2017. A high-accuracy map of global terrain elevations. Geophys. Res. Lett. 44 (11), 5844–5853.
Zhang, X., Ji, X., Li, C., Yang, T., Huang, J., Zhao, Y., Wu, Y., Ma, S., Pang, Y., Huang, Y., He, Y., 2022. A late Pleistocene human genome from southwest China. Curr. Biol. 32 (14), 3095–3109.
Zubova, A.V., Chikisheva, T.A., Shunkov, M.V., 2017. The morphology of permanent molars from the Paleolithic layers of Denisova Cave. Archaeol. Ethnol. Anthropol. Eurasia 45 (1), 121–134.